In presenting the dissertation as a partial fulfillment of the requirements for an advanced degree from the Georgia Institute of Technology, I agree that the Library of the Institute shall make it available for inspection and circulation in accordance with its regulations governing materials of this type. I agree that permission to copy from, or to publish from, this dissertation may be granted by the professor under whose direction it was written, or, in his absence, by the Dean of the Graduate Division when such copying or publication is solely for scholarly purposes and does not involve potential financial gain. It is understood that any copying from, or publication of, this dissertation which involves potential financial gain will not be allowed without written permission.

_____

7/25/68

AN INVESTIGATION OF METAL PARTICLE REACTION WITH THE SODIUM D LINE REVERSAL TECHNIQUE

A THESIS

Presented to

The Faculty of the Graduate Division

by

Michael O. Schliessmann

In Partial Fulfillment

of the Requirements for the Degree

Master of Science in Mechanical Engineering

Georgia Institute of Technology

August, 1972

AN INVESTIGATION OF METAL PARTICLE REACTION

WITH THE SODIUM D LINE REVERSAL TECHNIQUE

Approved:

Chairman

Date approved by Chairman: 9/8/1972

ACKNOWLEDGMENTS

I wish to express my appreciation to those individuals who have contributed to my professional development. Special thanks are extended to Dr. P. Durbetaki, who suggested the problem of this thesis and whose help as thesis advisor guided and encouraged its preparation. I wish also to thank the other members of my thesis committee, Drs. S. V. Shelton and W. C. Strahle, for their review of this work.

I am also indebted to the technical assistance of Mr. Louis A. Cavalli and Mr. Joseph G. Doyal, who aided in the design and fabrication of the laboratory equipment.

Finally, I would like to thank my parents for their concern and understanding in the pursuance of my education.

TABLE OF CONTENTS

Page

LIST OF TABLES

LIST OF ILLUSTRATIONS

LIST OF ILLUSTRATIONS (Continued)

NOMENCLATURE

Symbol	
g	Number of Degenerate States
k	Stephan-Boltzman Constant
$\overline{K.E.}$	Average Kinetic Energy
N	Number of Particles
$N(\lambda,T)$	Spectral Radiance
P	Absolute Pressure
Q	Heat
T	Absolute Temperature
T_b	Brightness Temperature
V	Volume Flow Rate
X	Molecular Weight
x,y,z	Flow Coefficients
$\alpha(\lambda,T)$	Spectral Absorptance
λ	Wavelength

Subscript	
a	Refers to Thermal Radiator a
a	Refers to Flow Conditions at Time of Use
b	Refers to Flow Conditions at Time of Calibration
f	Refers to the Flame
j	Refers to the j energy level
k	Designates the kth Mode of Internal Energy Storage

NOMENCLATURE (Continued)

Subscript

1	Refers to the Reference Lamp
1f	Refers to the Combined Effects of the Lamp and the Flame
o	Refers to the Entire System

Superscript

b	Designates a Blackbody Radiator

SUMMARY

The high heats of reaction of the light metals have led to their consideration as performance additives to liquid and solid propellants. But the ignition characteristics of metals are poorly understood and performance of these fuels has fallen far short of expectations.

This work is an investigation of the reaction behavior of 19 micrometer aluminum particles, 35 micrometer aluminum particles, and 50 micrometer magnesium particles in high temperature flames. A welding torch has been modified to allow the introduction of these particles by a nitrogen carrier stream into a methane oxygen flame. The effect of the particle reaction on the flame temperature was determined by the sodium D line reversal technique. The objective of this work was to carry out preliminary testing of the apparatus and to assess the capabilities and limitations of the system with regard to its applicability to metal ignition research.

The flow of the reactant gases supporting the flame was varied to allow evaluation of the effects of flame temperature and oxygen/fuel ratio on the metal particle behavior. Several regions of the flame were examined to determine the relationship between particle residence time and the mode of metal reaction.

The results of the introduction of magnesium particles and the smaller aluminum particles indicate reaction on the surface of the particles in a flame limited by the diffusion of liquid metal

from the core of the particles outward to the particle surface. The data taken in observation of the reaction of the larger aluminum particles is inconsistent with the data of the other two particles and suggests the possibility of errors in temperature determination caused by the scattering of reference radiation by these particles.

CHAPTER I

INTRODUCTION

Thermodynamic considerations have led to the study of the combustion characteristics of low molecular weight metals. Figure 1 illustrates a comparison of the heats of reaction of two conventional fuels, carbon and aviation kerosene, with two of the light metals, beryllium and aluminum [1]. The high heats of reaction computed on a volumetric basis of these two metals has led to their inclusion in propellants as high performance additives. However, due to incomplete combustion of these metal additives the improvement in performance of these propulsion fuels has fallen far short of expectations. The practical problem of improving propellant efficiency coupled with purely scientific interest has led to detailed study of the reaction and ignition characteristics of metals.

A. Background

A literature survey of recent work in the field of metal ignition has been prepared by Shakill [2]. His survey extends across the spectrum of heterogeneous combustion including various means of ignition, types and configurations of fuel to be burned. This present work will include only a basic outline of the leading theories proposed governing the ignition of small metal particles in a high temperature flame region. For a more complete bibliography, Shakill's work is referred to.

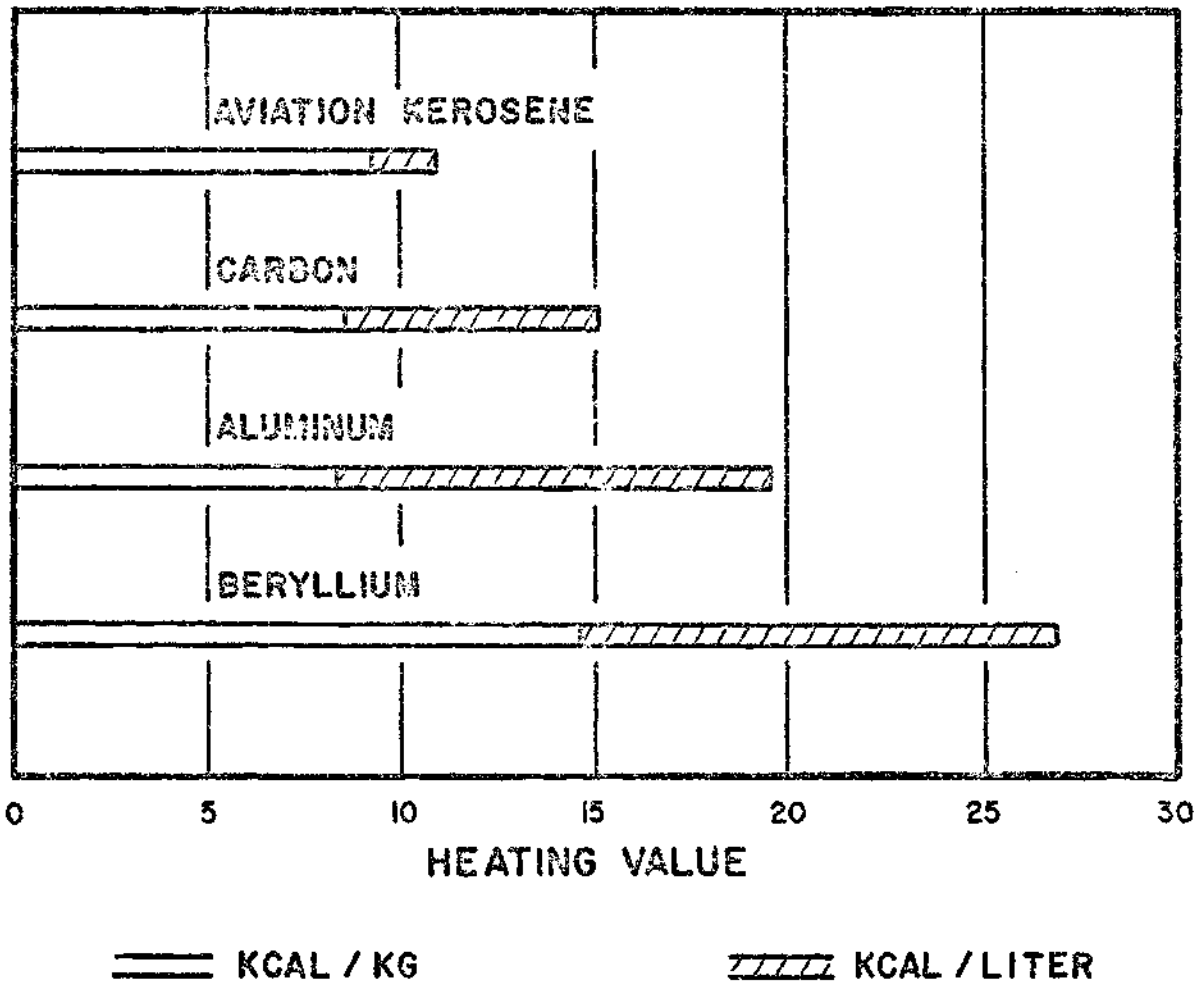

Figure 1. Heating Values of Several Fuels.

No precise model for metal particle burning thus far proposed has met with general acceptance. Experiemental confirmation of theory has been hampered by a lack of extensive, reliable thermodynamic information concerning the metals of interest and their oxides [3, 4]. As has been noted [5], not even the relative magnitudes of the boiling point and melting point temperatures of certain metals and their oxides have been established. It will be noted that these boiling points represent a significant criteria in determining the mode of ignition.

For aluminum, the melting and boiling point temperatures of the metal and the oxide are particularly important. When exposed to the atmosphere aluminum will react on the surface and an oxide layer will be formed. The ratio of the volume of aluminum oxide to the volume of the aluminum which forms the oxide is very nearly one. This number is often referred to as the Pilling and Bedworth ratio. A value for this ratio of less than one would indicate that a porous oxide layer will be formed, allowing further oxidation. If this ratio is much greater than one, on the order of three, an oxide layer will be formed which would have the tendency to crack and peel away from the metal surface.

With combustion in mind, where oxidation is desirable, either of these two conditions would be preferable to aluminum's Pilling and Bedworth ratio of 1.4. Because the oxide is very nearly the same volume as the aluminum from which it is formed, a protective layer is built up which effectively shields the aluminum from further reaction. The formation of this layer makes aluminum an ideal structural material with few corrosion problems but poses serious difficulties in its utilization

as a fuel. Coupled with high melting and boiling points of the oxide, this shielding necessitates a complex model governing aluminum particle ignition.

Experimental work illustrates the involved nature of aluminum combustion [6, 7, 8]. Small aluminum particles were exposed to flames of a variety of fuels with varying conditions of flame temperature and particle residence time within the flame. In some cases, the combustion process was interrupted; the particles were quenched and removed from the flame. In others the particles were allowed to proceed undisturbed through the flame region and were later collected.

Microscopic examination of the particles revealed three general configurations resulting from exposure to the flame. A high percentage of the aluminum particles apparently failed to react in any manner. They appeared, as before introduction into the flame, as small aluminum spheres. Also observed were small solid spheres of aluminum oxide. A significant number of large hollow spheres of aluminum oxide were also noted. These large, thin-walled spheres were found in many cases to measure of twice the diameter of the original aluminum particles. No significant correlation between the resultant particle configuration and the flame temperatures or particle residence times was apparent. In fact, a further complication was introduced. The formation of the large oxide shells seemed to be more frequent when hydrogen and oxygen were used to support the flame than when a hydrocarbon and oxygen supplied the flame.

A mathematical model has been proposed for the high temperature ignition of aluminum particles which predicts in some cases the formation of hollow oxide spheres [9]. Additional oxidation of the particles by

water vapor in the hydrogen-oxygen flame is thought to be responsible for the increased frequency of their formation.

Thomas A. Brzustowski and Irvin Glassman have proposed a broad qualitative model applicable to the ignition of particles in general [5]. As applied to aluminum, the predicted reaction modes number four, depending upon the particle temperature. If the temperature of the particle is below the melting point of aluminum, 932^{o}K, a surface layer of aluminum oxide will be formed. No further reaction will occur. For the particle temperatures above the melting point of aluminum but below the melting point of the oxide, 2318^{o}K, the shielding layer of oxide formed is thicker, but the bulk of the aluminum in the particle does not oxidize. In the temperature range above the melting point of the oxide but below its boiling point, 3800^{o}K, a molten layer of oxide is formed on the surface of the particle. This liquid shell allows aluminum from the core of the particle to diffuse outward and oxidize on the surface. If the reaction is allowed to proceed to completion a small solid sphere of aluminum oxide will result.

Theories diverge at this point and for the mode of reaction at temperatures above the boiling point of the oxide with regard to the formation of the large, hollow oxide spheres. A vapor phase reaction is predicted in this temperature range as opposed to the surface burning characteristic of lower temperatures. The model is initially the same as that governing the combustion of a hydrocarbon droplet. Aluminum is vaporized at the surface of the particle and diffuses outward into the oxidizing environment. Gaseous aluminum oxide is formed in a flame located some distance from the particle. But, unlike the products of

combustion of the hydrocarbon droplet, the oxide formed tends to condense as it moves from the flame front. If the oxide diffuses outward from the particle it could condense into very small oxide spheres and appear as the "smoke mantle" noted by C. M. Drew et al [8, page 19]. If, on the other hand, diffusion occurs inward toward the particle, the oxide could condense into large molten shells. After removal from the flame, these would cool and solidify into the thin walled oxide spheres reported by experimentists. The mathematical model cited earlier does predict this. But precision photographic techniques have indicated a complex bubble blowing process forming these spheres. A case can be made for the theory that they are formed from molten aluminum oxide in the surface burning mode. The boiling point of pure aluminum, 2740^{o}K, is far below the boiling point of its oxide. Vaporization of aluminum from the surface could lift the molten oxide layer and thus form an oxide shell some distance out from the particle.

The lack of correlation of theoretical predictions with the experimental results indicates the need of further experimental work in the field of metal ignition. The establishment of precise models predicting particle ignition behavior in general could result not only in the development of higher performance propellants but could also lead to a better understanding of the factors involved with the fire hazards of dust clouds and aid in the industrial treatment of particulate emissions.

B. Statement of the Problem

It was decided to approach the field of metal combustion from the macroscopic standpoint of the effect of the reaction of a cloud of metal particles on the temperature of the flame. A literature search revealed that most of the work performed in this field centered around the study of single particle ignition. Some research involving aluminum dust clouds has been performed here at the Georgia Institute of Technology. Mohammad Amin Shakill constructed a flat flame burner with an opposed jet of nitrogen carried aluminum particles [2]. His opposed jet arrangement permitted longer residence times of the aluminum particles in the flame region than is possible with the more conventional parallel flow configuration. Working with a thermocouple probe precisely positioned by a DISA sweep drive mechanism, Clarence A. Fisk plotted temperature profiles for a variety of fuel-air and aluminum particle reactions on this burner [10].

One significant drawback to Shakill's burner is that it is air cooled and flame temperatures in excess of the melting point of aluminum oxide could not be achieved without overheating the burner. A burner was desired with flame temperature capabilities ranging from below the melting point of the oxide to above its boiling temperature. Because of the corrosive nature of high temperature flames, a different method of temperature determination would also be beneficial.

To this end an oxy-acetylene welding torch has been slightly modified to allow its use in combustion work. Temperature determination was accomplished optically by the sodium D line reversal technique. The advantage of optical temperature determination over probe thermometry lies

not only in bypassing the problem of thermocouple destruction or catalyctic reaction in the flame or in avoiding gas flow disturbance by the probe. The temperature error due to radiative exchange between the thermocouple and the cooler environment is avoided entirely. The premixed flames used here have very low optical density and ordinarily temperature correction for this radiation loss is comparatively simple. But the introduction of an aluminum dust cloud into the flame complicates the energy balance as the fine particles radiate considerable [11].

In addition, for the ranges associated with these flames, the International Practical Temperature Scale does not define temperature along the lines of a thermal equilibrium concept. For temperatures above the freezing point of gold, 1063.0°C, temperature is interpreted on the basis of monochromatic radiant intensity. This is the method used in employing the reversal technique.

The theory behind the sodium D line reversal method of temperature determination is discussed in some detail in Appendix I, but a brief description of its nature will be given here. Sodium is introduced into the flame and the resonant D lines emitted at 5889.0 Å and 5895.9 Å are observed with a monochromator. Light from a reference source is passed through the flame and its emission is observed as a continuous background upon which the two sodium lines are superimposed.

When the reference source is at a temperature lower than the flame the sodium lines appear brighter than the background. As the temperature of the reference source is raised, the sodium lines tend to merge into the continua. If the reference source is raised to a higher temperature

than the flame the sodium lines are reversed; that is, they appear darker than the background continua.

The sodium lines vanish completely and only the continua can be observed when the reference source and the flame are at the same temperature. Subject to certain limitations, which are noted in Appendix I, this null type measurement provides an extremely reliable means of determining flame temperature. The precision with which the temperature of the background source is determined represents the primary constraint to the accuracy of this technique.

This present work is limited in scope to the design and assembly of a system which would enable optical temperature measurement of particle ignition reactions. The investigation of various flames with metal powder seeding formed a basis for preliminary evaluation of this system's capabilities.

The reactions of magnesium particles and of two sizes of aluminum particles were examined. The complex model discussed governing aluminum particle reaction varies with particle size. The magnesium particles are predicted to undergo an accelerated reaction otherwise similar to that of the smaller aluminum particles.

As a continuation of research in the field of metal ignition it is expected that the apparatus assembled here will serve as a basis for future experiments, and it is hoped that the experience gained here will serve as a guide in planning future activities.

CHAPTER II

EQUIPMENT AND INSTRUMENTATION

A system incorporating the sodium D line reversal technique for temperature measurements of metal particle reactions requires three primary components: a high temperature region to serve as a reaction zone for the particles, a monochromator to resolve the D line emission, and a reference source whose temperature may be easily modulated. The system assembled here is illustrated in Figures 2 and 3. The flame of slightly modified welding torch provided the reaction zone. Supporting subsystems for the flame include a gas flow and metering system to control the flame and a powder feeder arrangement to introduce the metal powder to the flame. A diffraction grating spectrograph served as a monochromator and a tungsten strip filament lamp was used as the reference source. Additional features of the assembly are an optical arrangement for focusing the radiation from the reference source through the flame and to the monochromator and either electronic or visual monitoring of the D line emission.

A. The Torch

The spectrograph's size and lack of mobility dictated a flexible design of the remaining components of the particle ignition study system. An AIRCO oxy-acetylene welding torch was selected to support the flame. Dimensionally small and lightweight, it had the capability of being

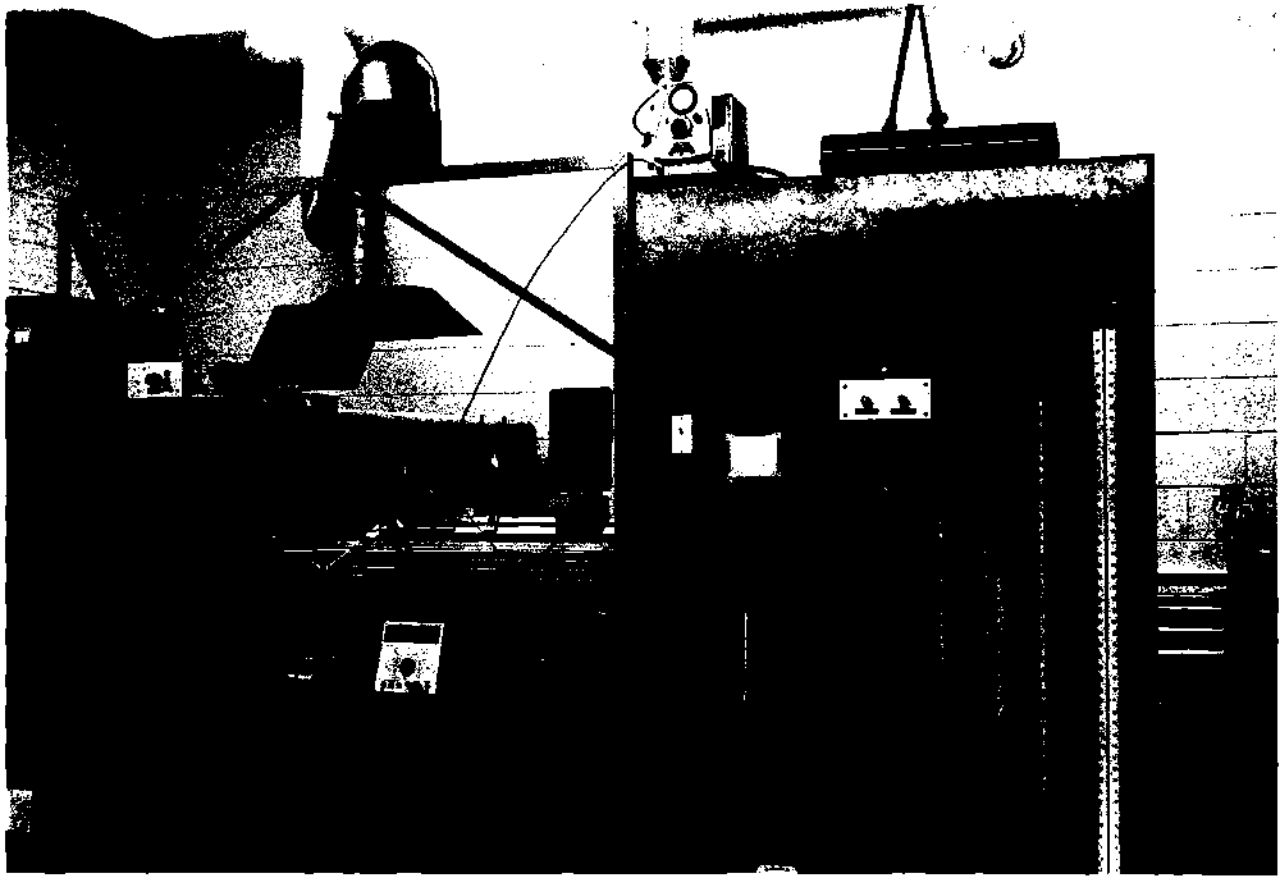

Figure 2. The Line Reversal System.

Figure 3. Close-Up of the Torch.

easily positioned with clamps attached by carriages to the optical bench of the spectrograph. The torch's flexible hose allowed the torch complete freedom of movement along this track. In addition, its simple design allowed for operation over a wide range of temperatures without the problem of over heating. In the present work oxygen and methane were used to support the flame. Nitrogen carried metal particles were introduced into the reactant gas flow stream through a length of 1/16 inch stainless steel tubing inserted through the wall of the torch tip and silver soldered in place. This particle injection occurred approximately seven inches upstream from the nozzle of the torch. The resulting symmetrical flame evidenced uniform mixing of the reactant gases with the particles and their nitrogen carrier. The orifice of the torch tip was 0.082 inches in diameter.

Originally the torch was secured to a carriage capable of sliding along the optical bench. Later, it was desired to study higher regions of the flame by lowering the torch. Here the pedestal of the carriage presented an obstacle and it was found necessary to position the torch with clamps attached to a vertical aluminum rod secured to the table. This allowed satisfactory vertical alignment of the desired portions of the flame with the aperture of the spectrograph. Lateral movement of the torch was restricted with this arrangement, but once the optical system was finalized this degree of freedom was superfluous.

Magnesium powder was obtained from Hart Metals, Inc. which consisted of spherical particles with an average diameter of 50 micrometers (200/320 mesh). Alcan Metal Powders supplied two sizes of aluminum

powder: one with an average particle size of 19 micrometers, the other with an average particle size of 35 micrometers. Particle size distributions within these powders is given in Appendix V.

Metal particles were introduced into the carrier nitrogen stream by a METCo Type 3MF powder feed unit. Designed to provide an extremely high mass flow rate of the particles, this unit required modification for its use in the present work. The alteration of the discharge nozzle by Fisk [10] was incorporated here. In addition, the bucket wheel was removed entirely and the gas distributor plug supplied by the manufacturer was replaced by one which extended down beyond the bucket wheel compartment. See Figure 4. This compartment then served as a reservoir for the particles. The gravity fed particles entered the nitrogen stream in the modified gas distributor plug through a hole drilled in the plug inclined approximately 45° from the vertical. Several of these plugs were machined from a cast plexiglas rod and by varying the hole diameters a satisfactory range of particle flow rates could be obtained. A fairly uniform powder flow of the larger--35 micrometer average diameter--aluminum particles resulted with the holes of the dimensions given in Figure 4. Cohesion of the smaller--19 micrometer average diameter--necessitated enlargement of these holes for a uniform flow. This arrangement, however, was found to be unsatisfactory for the coarser 50 micrometer magnesium particles. For these particles the manufacturer's own gas distributor plug was used. This plug offers no restriction to the powder flow, and at the same time no problem of dumping large quantities of magnesium into the carrier flow was encountered.

The powder feeder unit was located on top of the flame control

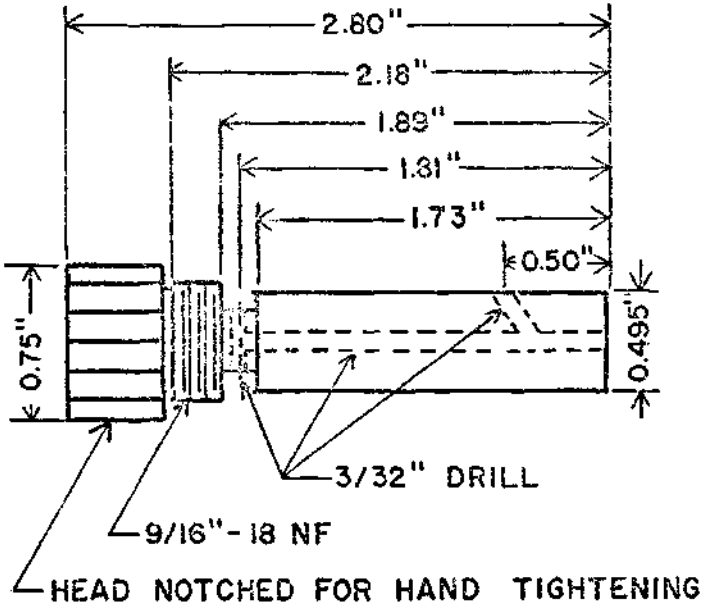

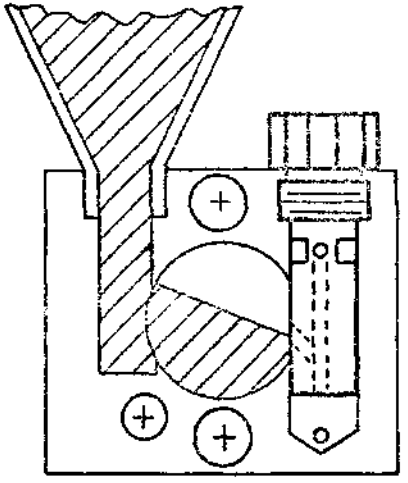

Figure 4. Modified Gas Distributor Plug.

board approximately three feet above the torch. Tubing from this unit to the torch was arranged so that flow of the particles in the nitrogen carrier stream against gravity was avoided. Electric vibration of the tubing from the powder feeder to the torch was tried but with little effect on the uniformity of the particle flow. Accumulation of the powder in this line is not a problem.

Figure 5 shows the flow of gases to the burner. High pressure cylinders fitted with two stage pressure regulators supplied the oxygen, methane, and nitrogen. One quarter inch copper tubing carried the methane and nitrogen to the flowmeters. Oxygen was channeled through 5/16 inch rubber hose. Pressure downstream of the flowmeters was monitored with manometers. The methane and oxygen then flowed through needle valves equipped with micrometer scales. These valves allowed a precision in flow adjustment not attainable with the valves integral to the flowmeters. Temperature was then determined by the flow of these gases through thermometer wells. From these wells standard oxygen and acetylene hoses carried the reactants to the torch.

Nitrogen flow downstream of the manometer tap was split into a carrier system and a bypass system. The carrier system led the flow through the powder feeder and down via 1/8 inch copper tubing to the torch tip. The bypass system carried the flow directly to the torch. Needle valves in each of these systems provided for not only closing a system completely but also proportioning the flow between these two systems.

Two methods were tested to introduce sodium to the flame. In the first method finely crushed salt was mixed with the metal powder and taken to the flame by the carrier nitrogen flow. Salt dilution of

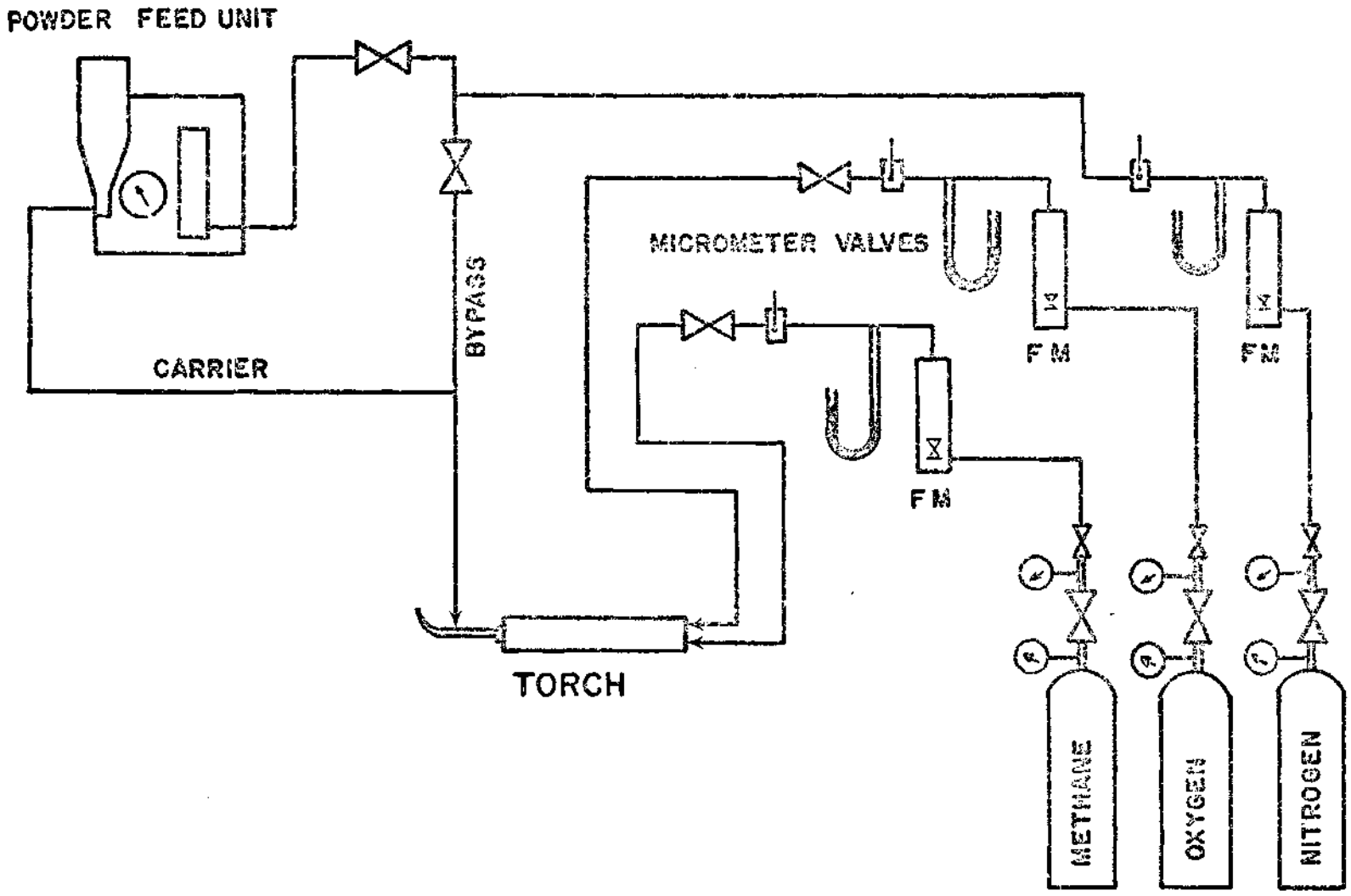

Figure 5. Gas Flow and Metering.

the metal powder was not significant. A ratio of about 400 to one on a weight basis of the metal powder to the salt provided strong enough sodium lines to accomplish reversal. Sodium seeding of the flame without the addition of metal particles required the removal of the metal particles from the feeder unit. Crushed salt was placed in the unit and again carried to the flame by nitrogen. In this case, however, it was found necessary to run a large proportion of the nitrogen flow through the bypass system to avoid having large quantities of salt delivered to the flame. Even an extreme mass flow rate of the salt would not significantly affect the temperature of the flame, but problems associated with self reversal of the D line emission would be increased. The difficulties posed by self reversal are discussed in Appendix I.

A fine salt water mist was used in the second method. Nitrogen from an auxilliary high pressure cylinder was passed through a spray atomizer which created a fine mist. The atomizer and its salt water reservoir were located in a closed ten gallon water bottle. An outlet tube near the top of the bottle enabled collection of the smaller droplets of the mist. This mist was carried through flexible tubing to a nozzle at the torch tip. The nozzle consisted of a conical section of heavy plastic which was fitted over the torch tip.

A high nitrogen flow rate was required to supply the flame with sufficient sodium for the reversal phenomena to be easily observed. This high flow rate tended to blow the flame off the torch tip, and successful utilization of this method of salt introduction was possible

only for high flow rates of lean flame mixtures. Additionally, comparison of the flame temperatures using this method of sodium introduction with temperatures recorded by placing a small amount of salt on the nozzle of the welding tip revealed a 90°C or more decrease in temperature for the same flame. This temperature drop is thought to have been due primarily to nitrogen dilution of the reactant flow as a decrease of 15°C or less is expected to be caused by the water droplets in the mist [12].

The spray mist method held the advantages of shielding the flame to some extent from the room environment and providing salt introduction independent of flow and powder feed settings, but because of stable flame limits restricting operations to high flow lean mixtures this method was discarded. The first method of introducing the sodium by the carrier nitrogen flow produced generally satisfactory results.

B. The Monochromator

A Bausch and Lomb two meter spectrograph was used as a monochromator. For this work, the instrument was fitted with a diffraction grating scribed with 1200 lines per millimeter for electronic measurements and with one of 600 lines per millimeter for visual monitoring. The former grating will provide a first order dispersion of approximately four Angstroms per millimeter at the focal plane while the latter yields a first order dispersion of eight Angstroms per millimeter. An actual resolving power, $\lambda/\Delta\lambda$ of over 165,000 is predicted for a second order dispersion from the 1200 lines per millimeter grating.

This spectrograph was modified to some extent by Doty [13] to make it more suitable for combustion study. He replaced the original dovetail

slide optical bench with a standard Zeiss triangular type to allow the use of a larger variety of carriages and clamps. The manual drive linkage for the grating turret was modified to allow a constant angular velocity rotation of the grating by a synchronous motor. In addition, he designed the circuitry for and fitted two ten stage photomultiplier tubes into the spectrograph's photographic plate mount. The system he devised allowed by means of the constant velocity grating rotation the sweeping of the entire spectrum past the slits of the photomultiplier tubes. Outputs from these tubes were amplified and sent to a strip chart recorder. A relative intensity versus wavelength graph for the emission of the source monitored was the result.

Because of the physical size of the spectrograph, the torch, reference source, and supporting accessories were necessarily designed to accommodate it. The most extensive modification of Doty's system consisted of replacing his grating drive mechanism which was located by clamps directly in front of the spectrograph's control panel with an assembly mounted permanently to the top of the spectrograph's housing. The altering of the grating drive mechanism allowed easy access to the instrument's controls and provided space for the positioning of the torch near the slit jaws of the spectrograph.

A further modification to the spectrograph's photographic plate holder mounts was found necessary when it was attempted to align the slits of the photomultiplier tube assembly with sodium D lines from the flame. There was too much play in the linkage for these resonance lines to be centered precisely at the slits by the grating drive assembly.

A depth gage fitted with micrometer scales was attached to the plate holder stop of the spectrograph's mountings. The sodium D lines were positioned near the photomultiplier tube slits by the grating drive mechanism. Final alignment was accomplished by advancing the depth gage aginst the photomultiplier assembly with a maximum output from the tubes was recorded.

Visual determinations of line reversal conditions were made with a seven power magnifier affixed to the viewing plate over the line images.

Electronic measurements using the photomultiplier tubes and amplification circuitry were found to be less satisfactory than visual monitoring. This was due to the large response time for the system and severe dark current drift. Hence, the data presented in Chapter IV is the result of visual detection of reversal only. A discussion of the technique in applying the photomultiplier tubes to line reversal temperature measurement is given in Appendix III.

Apart from the changes listed above the system assembled by Doty was unaltered. A more complete description of his original apparatus together with an evaluation of its performance may be found in his thesis.

C. The Reference Source

A General Electric microscope illuminator lamp (18A/T10/1P-6V) with a prefocused base was used as a reference light source. Its base secured to a bench carriage, the lamp was positioned behind the flame on the optical track. A system of lenses was required to first focus the radiation from the lamp into the flame and then collimate the light from both the flame and the lamp onto the slit jaws of the spectrograph.

The system used is the one recommended by Thomas [14] and is shown in Figure 6.

Lens A is positioned to form an image of the filament of the lamp in the flame. Lens B then forms the image of both the flame and the lamp on the slit of the spectrograph. An aperture stop is located where Lens B would form the image of Lens A. Its purpose is to restrict the aperture such that the solid angle of light taken from the flame is the same as the solid angle taken from the image of the lamp in the flame. The absence of this aperture stop or general errors in placement of the lenses would result in more radiation from the flame being incident upon the spectrograph's slit than from the reference source. This would lead to temperature readings above the true temperature because the lamp filament would have to be hotter to establish reversal.

Current to the lamp was supplied by a powerstat and the voltage across it was monitored with a digital voltmeter. The lamp was calibrated, input voltage versus filament brightness temperature, using a Pyrometer Instrument Co., Inc. micro-optical pyrometer. This pyrometer, however, is calibrated at a wavelength of 6500 Å. Of concern is the filament's brightness temperature of 5900 Å, the wavelength of the D line emission. Thus, a correction is required. Both the calibration curve for the lamp and the correction curve are included in Appendix V. Calibration of the lamp was made through Lens A to avoid temperature corrections later on due to reflection losses caused by this lens.

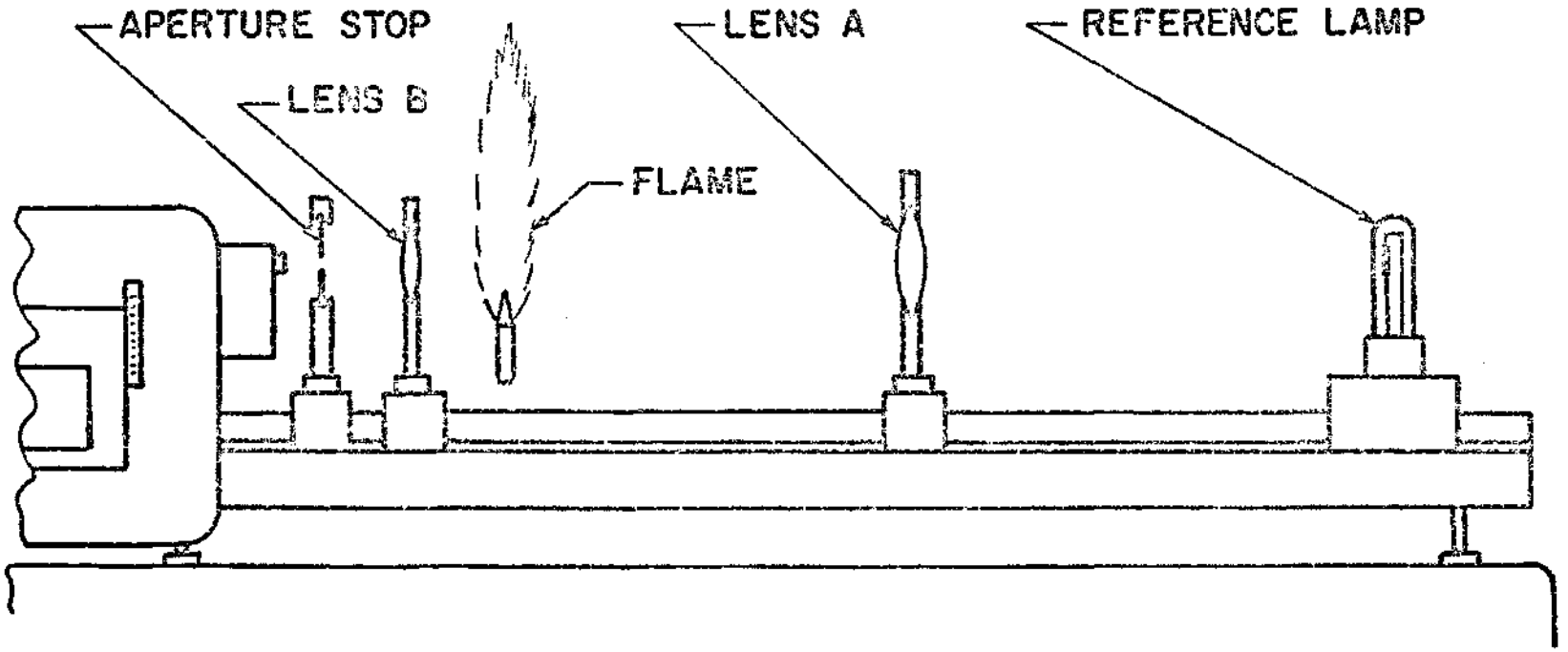

Figure 6. Optical System for Line Reversal.

CHAPTER III

PROCEDURE

As was noted in Chapter I, the mode of metal particle reaction is suspected to be strongly dependent upon the temperature of the particle. When these particles are introduced into a flame, the particle temperature becomes a function of the temperature of the flame and the duration for which the particle is exposed to this high temperature region. Further noted in the introduction was the apparent enhancement of particle reactions when the oxidizing species are increased.

It was desired to vary the three parameters: flame temperature, particle residence time, and availability of oxygen, in such a manner that the effect of each could be ascertained. To accomplish this, eleven flame mixtures were chosen for examination. These flames varied in adiabatic flame temperature, oxygen-fuel (o/f) ratio, and volume flow rate. By comparing flames of a given o/f ratio but varying the adiabatic flame temperature, the effect of flame temperature could be noted. Studying the particles at different heights above the torch tip provided a means of determining residence time effects. And variation of the o/f ratio for a constant volume flow rate of the reactant mixture enabled consideration of the oxygen availability parameter.

A. The Flame Mixtures

Figure 7 gives the stable flame limits for the torch with a nitrogen

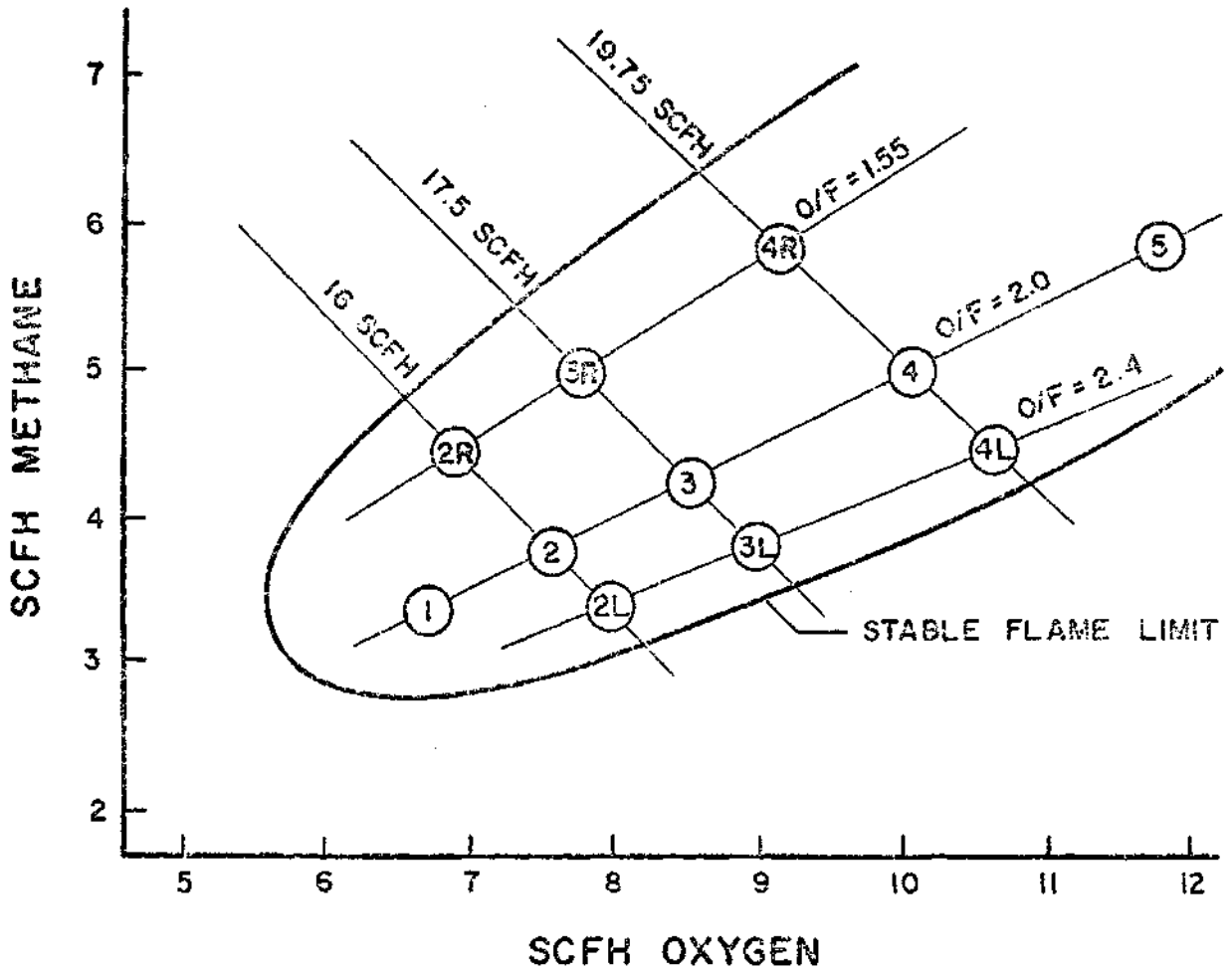

Figure 7. Torch Stability Limits and Flame MixturesChosen.

flow of 4.75 SCFH. A nitrogen flow of this magnitude or larger through the powder feed unit was found to be necessary to provide a uniform stream of metal particles to the flame. The numbered circles on the figure represent the mixtures chosen for study. Table 1 lists the adiabatic flame temperatures of each of these mixtures along with the reactant gas flow rates. Also listed are the approximate visible heights of each of these flames. Sample calculation of the adiabatic flame temperatures together with flowmeter corrections for non-standard temperature and pressure are given in Appendix IV.

Flame Nos. 1 through 5 are stoichiometric mixtures with increasing adiabatic flame temperatures. Flame Nos. 2R, 3R, and 4R are rich mixtures having the same volume flow rates as Flame Nos. 2, 3, and 4 respectively. Corresponding to these volume flow rates are also the lean mixtures of Flame Nos. 2L, 3L, and 4L.

A comparison of the particle reactions in Flame Nos. 1 through 5, 2R through 4R, or 2L through 4L yields adiabatic temperature effects for a constant o/f ratio. Similarly, the collated data from Flame Nos. 2R, 2, and 2L (3R, 3, 3L; 4R, 4, 4L) furnishes a basis for assessing the effect of the o/f ratio. Metal particle reaction in rich flames should be limited by the diffusion of oxygen from the atmosphere into the flame.

To study the particle residence time effects, the flame centerline region of each of these mixtures at three heights above the torch tip were considered. The regions studied were located 1.2 to 2.0, 1.8 to 2.6, and 2.5 to 3.3 inches above the torch tip. These regions were examined by raising or lowering the torch until the desired portion of the flame

Table 1. Specifications of the Flames Studied

Flame No.	Gas Flow (SCFH) CH_4	O_2	N_2	Adiabatic Flame Temperature (^oK)	Flame Height (inches)
1	3.32	6.64	4.75	4146	13
2	3.75	7.50	4.75	4247	14
3	4.25	8.50	4.75	4341	15
4	5.00	10.0	4.75	4456	16
5	5.85	11.7	4.75	4554	15
2R	4.41	6.84	4.75	3891	17
3R	5.00	7.75	4.75	3988	19
4R	5.89	9.11	4.75	4087	22
2L	3.31	7.94	4.75	3871	12
3L	3.75	9.00	4.75	3956	13
4L	4.42	10.6	4.75	4063	14

was correctly aligned with the aperture of the spectrograph and the optical system from the reference source. The region 2.5 to 3.3 inches above the torch tip was the highest portion of the flame that could be studied with the present arrangement because downward travel of the torch is limited by the presence of the optical bench. The region closest to the torch nozzle, 1.2 to 2.0 inches, was the lowest section of the flame that could be considered without including a portion of the inner cone.

It should be noted that the parameters of adiabatic flame temperature, o/f ratio, and particle residence time are not varied completely independent of one another. Increasing the volume flow rate of a given ratio of oxygen and methane will raise the adiabatic flame temperature because of the decreased percentage dilution by the carrier nitrogen. But the higher flow rate of the reactants causes a higher velocity of the metal particles in the flame and, hence, the particle residence time at a given height above the torch tip is affected. The residence time is not affected by changing the o/f ratio for a given volume flow rate, but the adiabatic flame temperature does change with these mixtures.

B. The Metal Particles

Three different metal powders were introduced via carrier nitrogen to the flame mixtures described above. Two of these consisted of aluminum spheres of different average diameters--19 micrometers and 35 micrometers. The third powder was of larger magnesium particles--50 micrometers in diameter. In physical appearance these powders differed considerably.

The larger diameter aluminum spheres and the magnesium particles were freely flowing while the smaller aluminum spheres exhibited cohesion to such an extent that the powder could be molded and shaped. Because of this and also the lack of a positive metering system within the powder feed unit, these particles were introduced to the flames at different mass flow rates. The larger aluminum were introduced to the flames at a rate of 4.85 grams per hour while the smaller aluminum particles and the magnesium powder was fed at rates of 1.61 and 0.162 grams per hour, respectively. These rates were determined by connecting a flask to the discharge line of the powder feed unit. The particles were trapped and collected in this flask. The change in weight of the flask over a given time interval of carrier gas flow provided the mass flow rates of each of the particles.

C. Temperature Measurement

Temperature readings were made by visual determination of the D line reversal condition. The torch was first aligned horizontally and vertically to expose the correct region of the flame to the optical system. Vertical adjustment was accomplished by attaching a scale to the torch tip. Power was supplied to the reference lamp and the torch height was adjusted until the image of the lamp filament was formed at the desired position on the scale. Sighting through the lamp and into the flame, the lateral position of the torch was adjusted until the lamp filament appeared centered in the flame. The reactant gas flow and powder feed rate were then adjusted to give the proper flame mixture.

After the flame mixture and torch position had been adjusted, the

spectrograph was used to view line reversal. Current to the reference lamp was increased until the brighter D lines from the flame disappeared into the background continua. At this point the voltage across the lamp was recorded. Then the lamp current was increased until the D lines were clearly reversed. The current was slowly decreased until the darker sodium lines merged again into the continua. Here the voltage was also recorded. The pair of voltages thus obtained bounded the reversal conditions for the flame and the lamp.

Temperature readings were taken at each of the three heights of all eleven flame mixtures for the introduction of each of the three metal powders and also for a fourth seeding of the flames with crushed salt only. The procedure of torch alignment, reactant flow metering, and reversal determination was repeated twice for each point. Thus, three pair of voltages bounding the reversal conditions at each flame height for each combination of flame mixture and metal powder resulted.

These six voltages were averaged to yield a voltage representative of the temperature of that region. The calibration curves for the lamp were then consulted to convert this voltage into filament brightness temperature. For the line reversal condition, this is equal to the flame temperature.

CHAPTER IV

EXPERIMENTAL RESULTS AND DISCUSSION

This investigation has as its primary result the effects of the introduction of streams of magnesium particles, 19 micrometer aluminum particles, and 35 micrometer aluminum particles on the temperature of methane oxygen flames of varying flow rates and oxygen fuel ratios. These results are presented in Figures 9 through 18 as plots of the centerline flame temperature versus the region height above the torch tip. Included on these figures is the temperature spread encountered during the data recording for each of the plotted points. Most of the readings lie within the temperature range designated by the size of the data points, $\pm 5^{o}$ C.

At this point, general trends will be noted from these plots of the effects of the parameters of flames temperature, particle residence time, and o/f ratio. These trends will be correlated with the anticipated behavior predicted by the general metal particle combustion model outlined in Chapter I. In addition, the method of examining the reaction behavior of the metal particles through line reversal temperature measurements as performed in this investigation will be evaluated. Finally, the reliability of the experimental results will be compared with the anticipated experimental error.

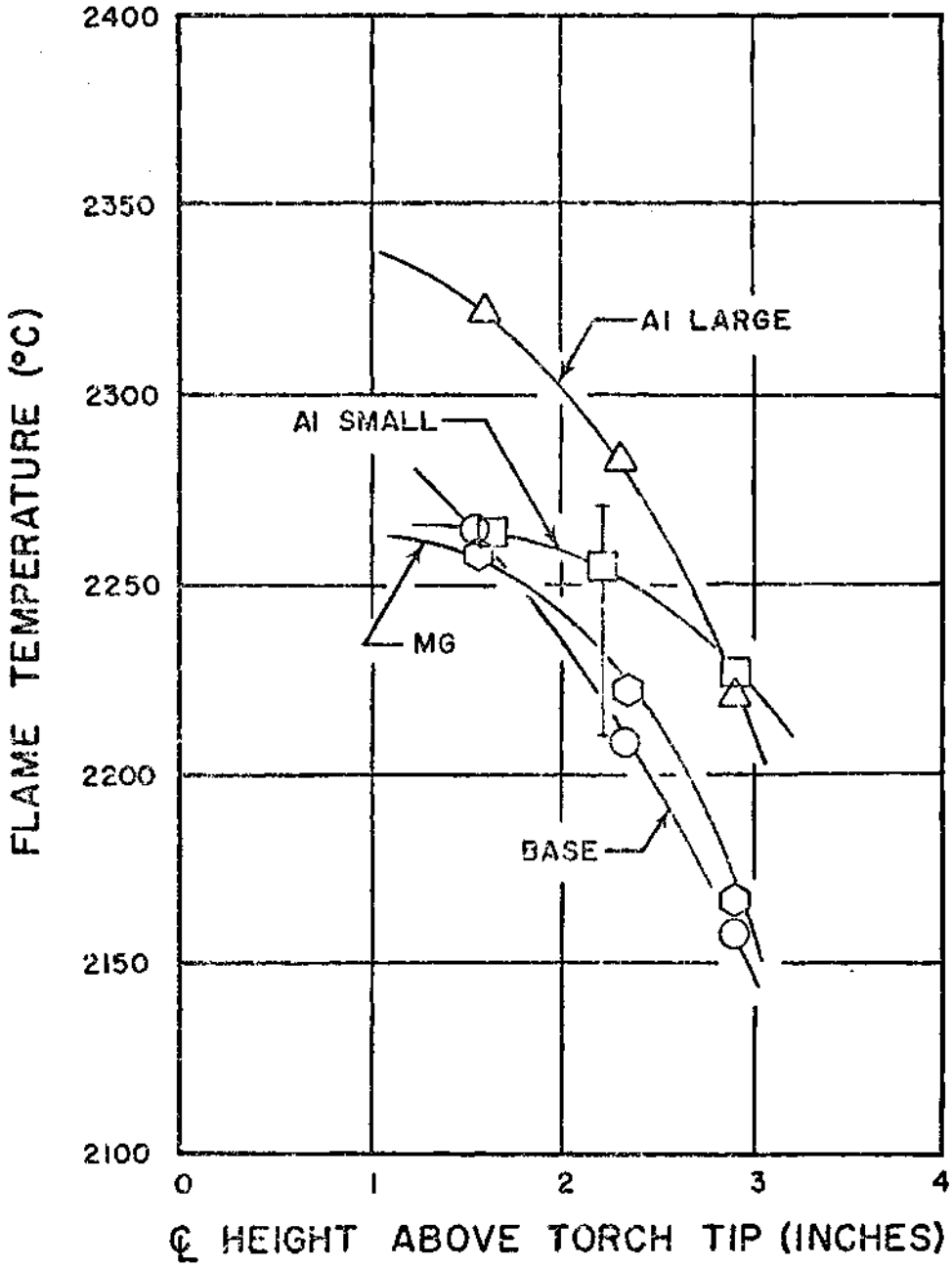

Figure 8. Temperatures of the Center Regions of Flame No. 1.

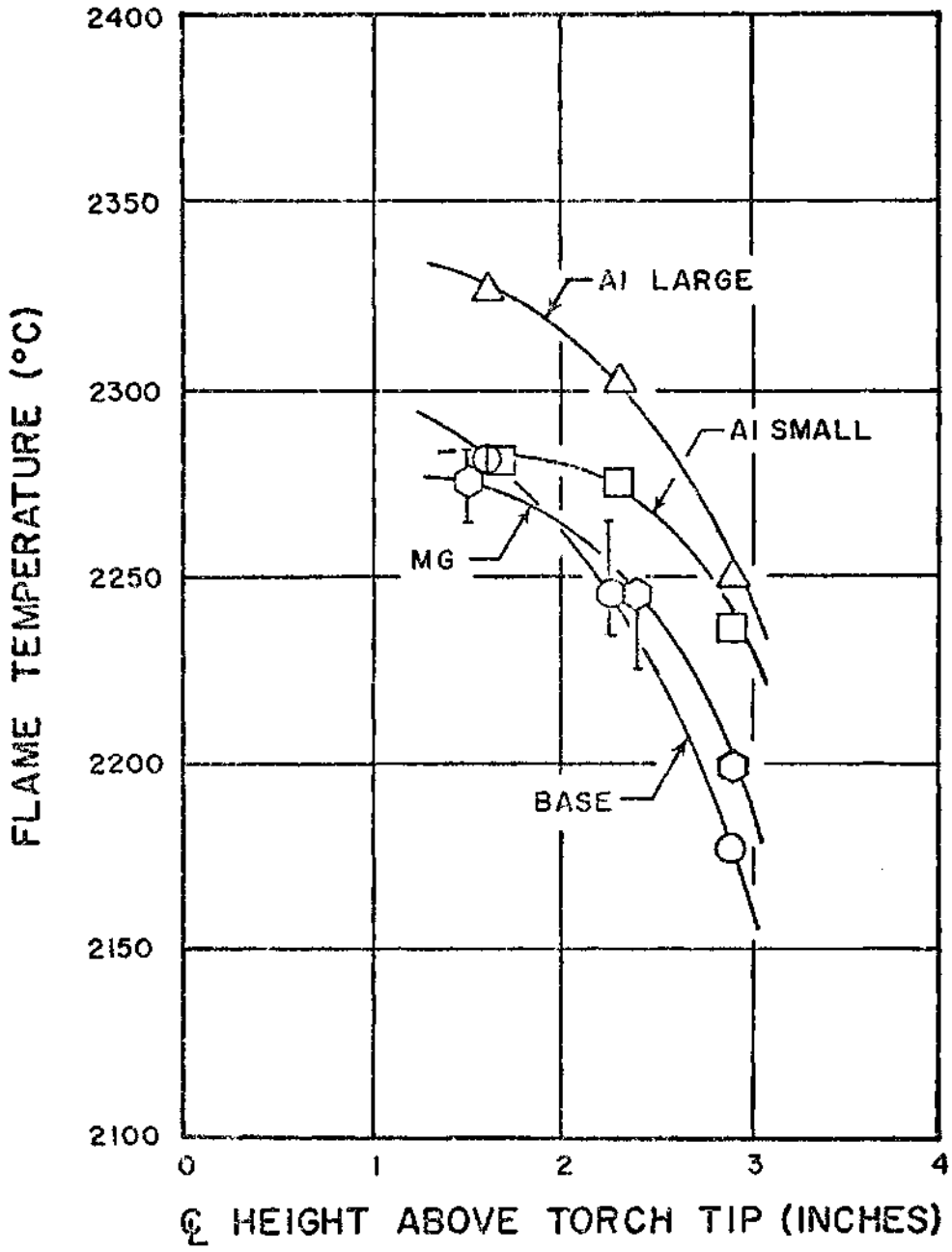

Figure 9. Temperatures of the Center Regions of Flame No. 2.

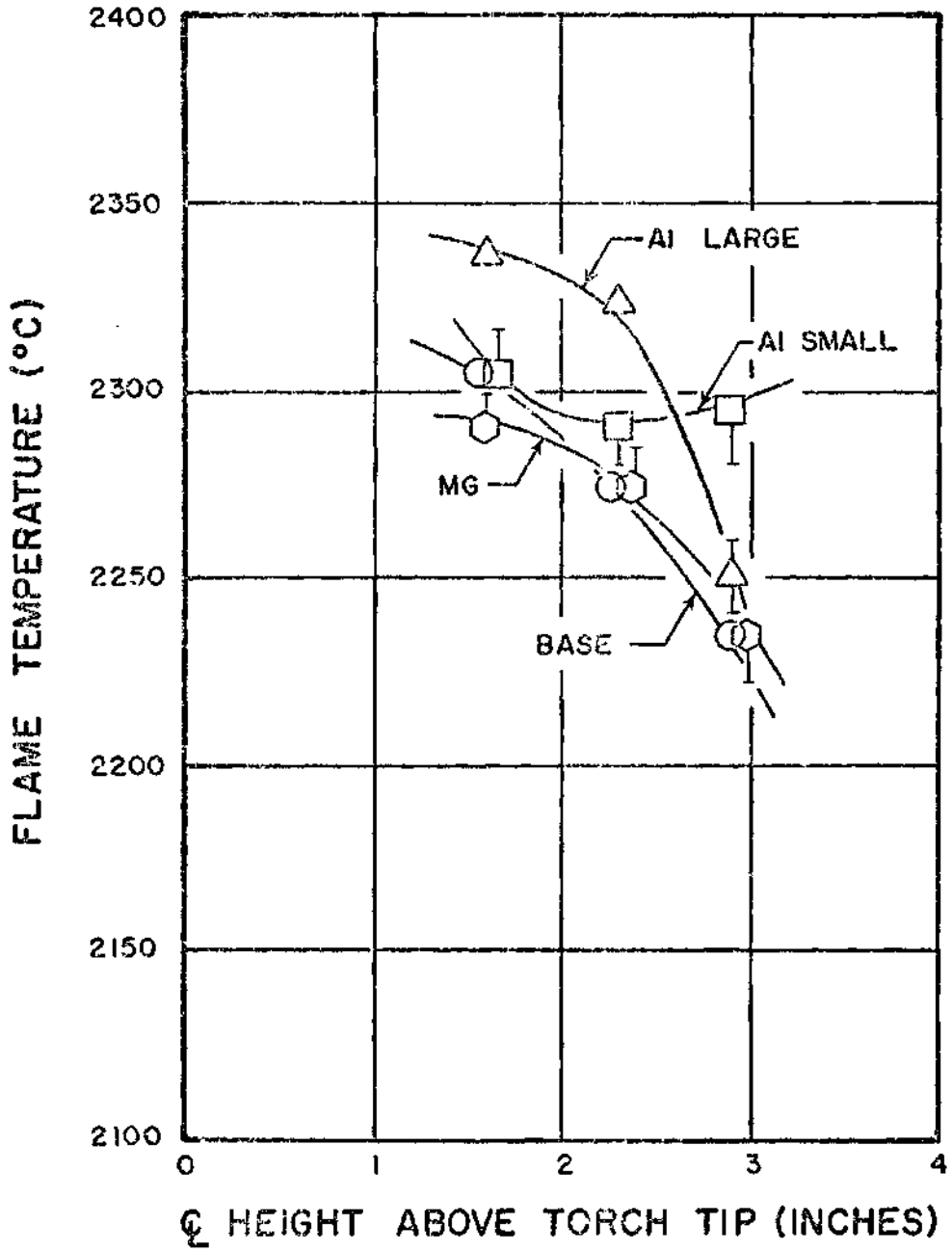

Figure 10. Temperatures of the Center Regions of Flame No. 3.

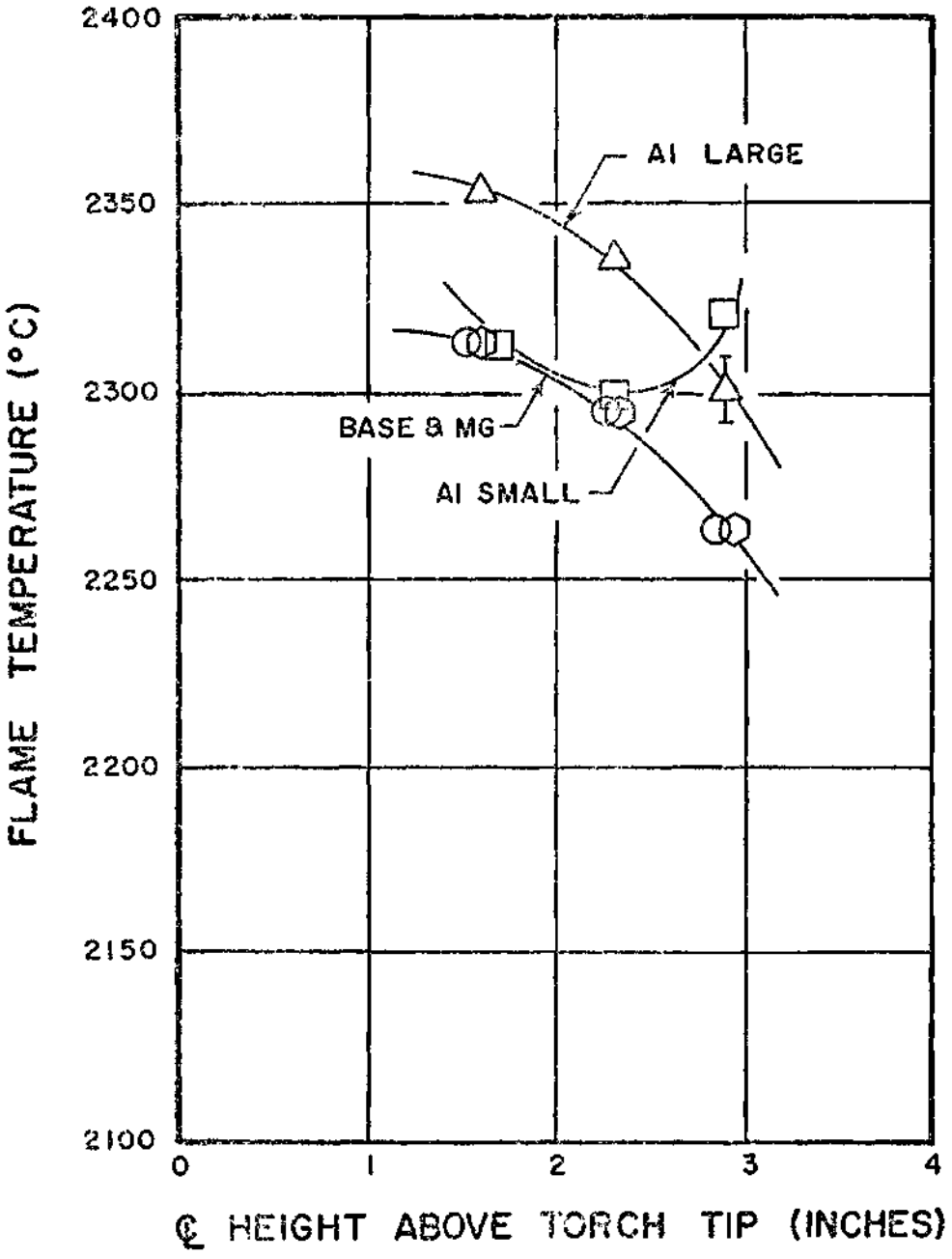

Figure 11. Temperatures of the Center Regions of Flame No. 4.

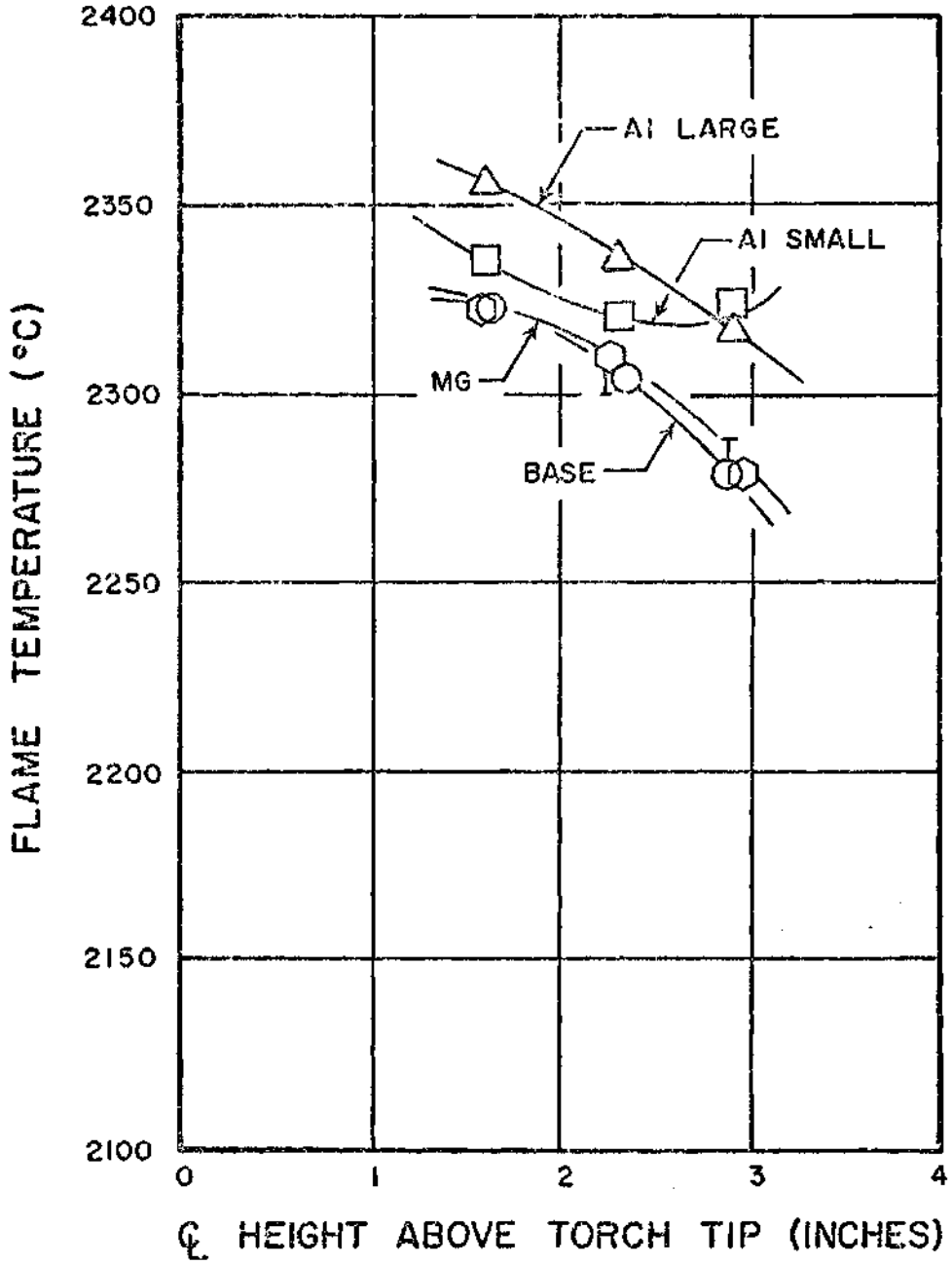

Figure 12. Temperatures of the Center Regions of Flame No. 5.

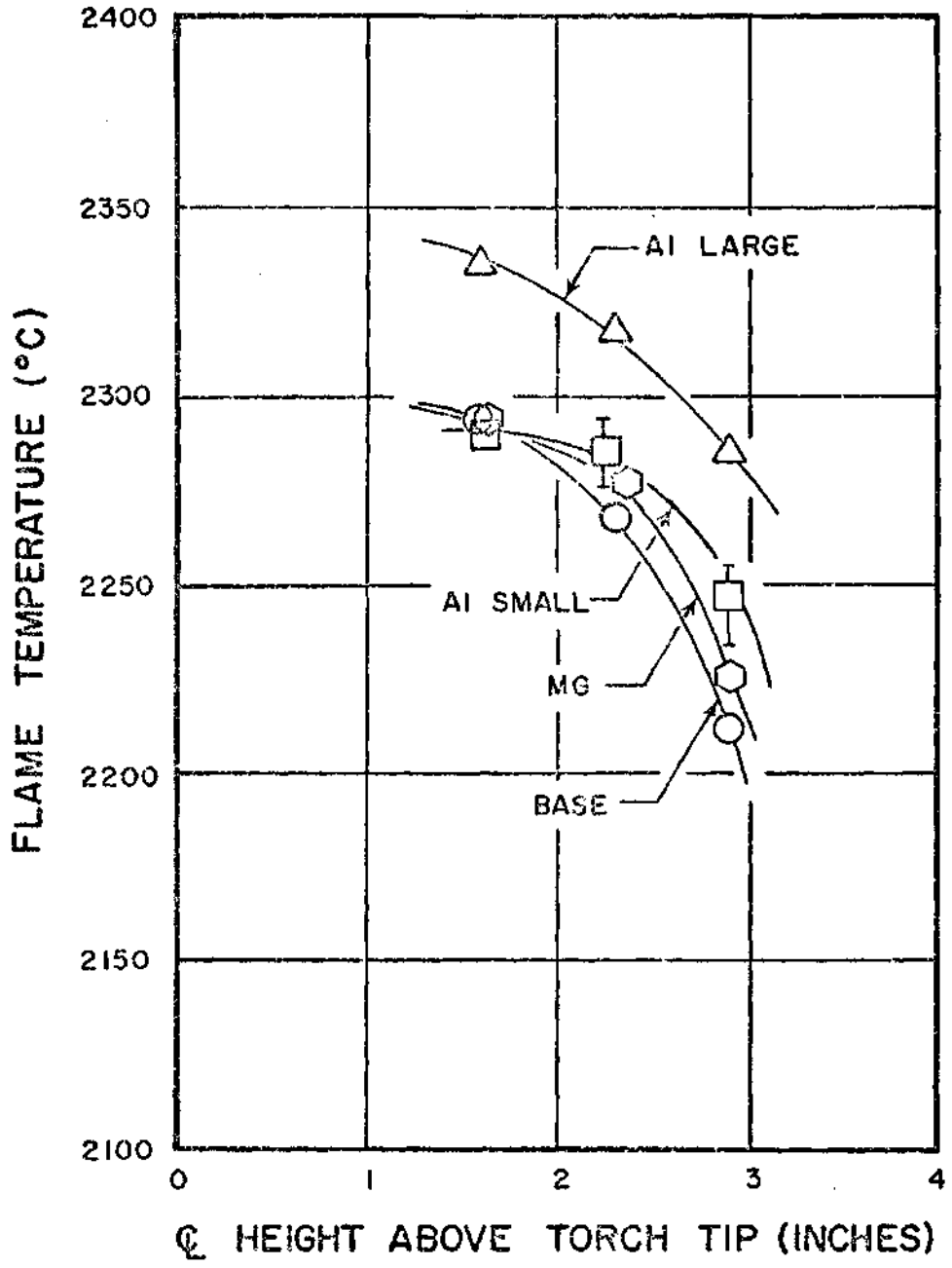

Figure 13. Temperatures of the Center Regions of Flame No. 2R.

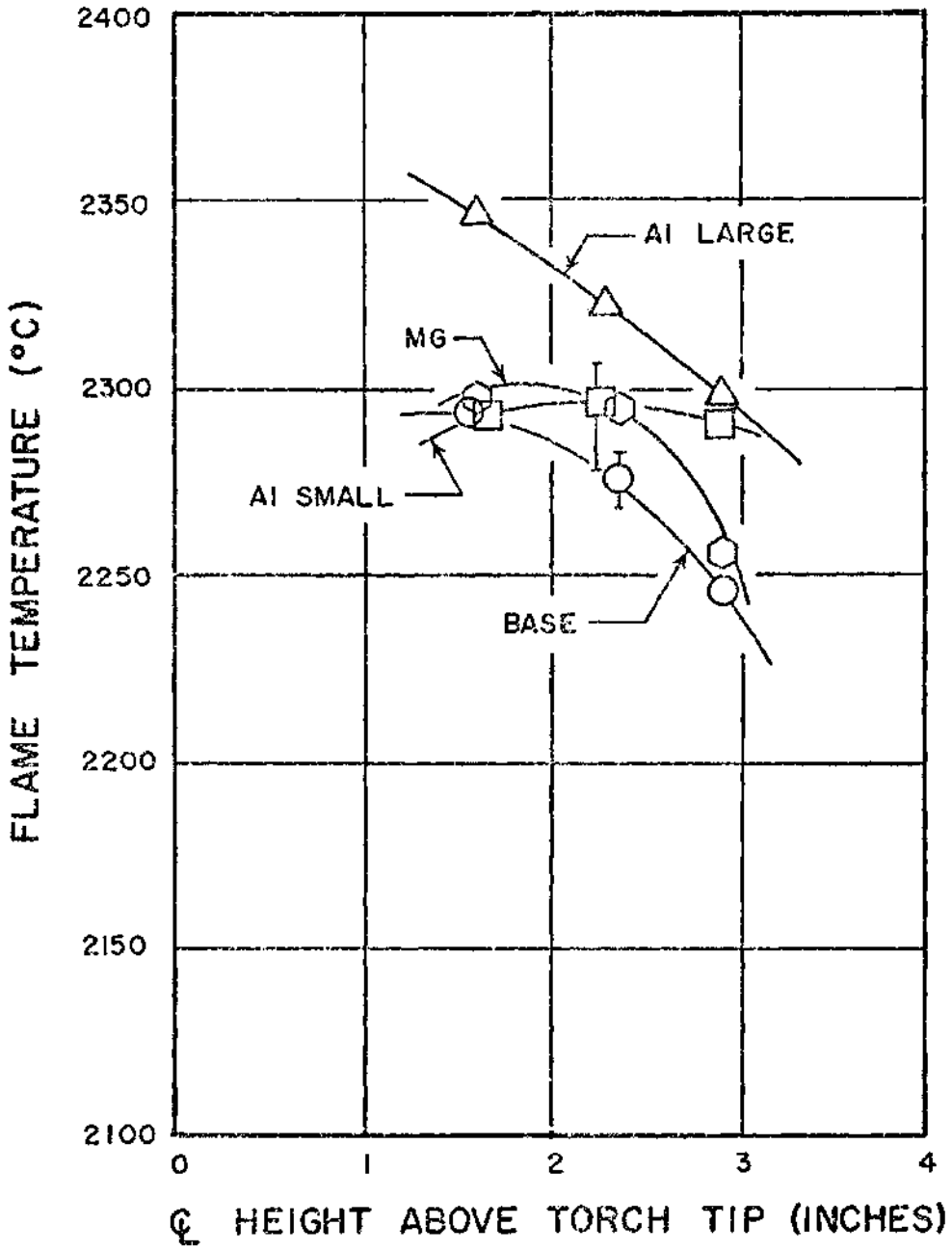

Figure 14. Temperatures of the Center Regions of Flame No. 3R.

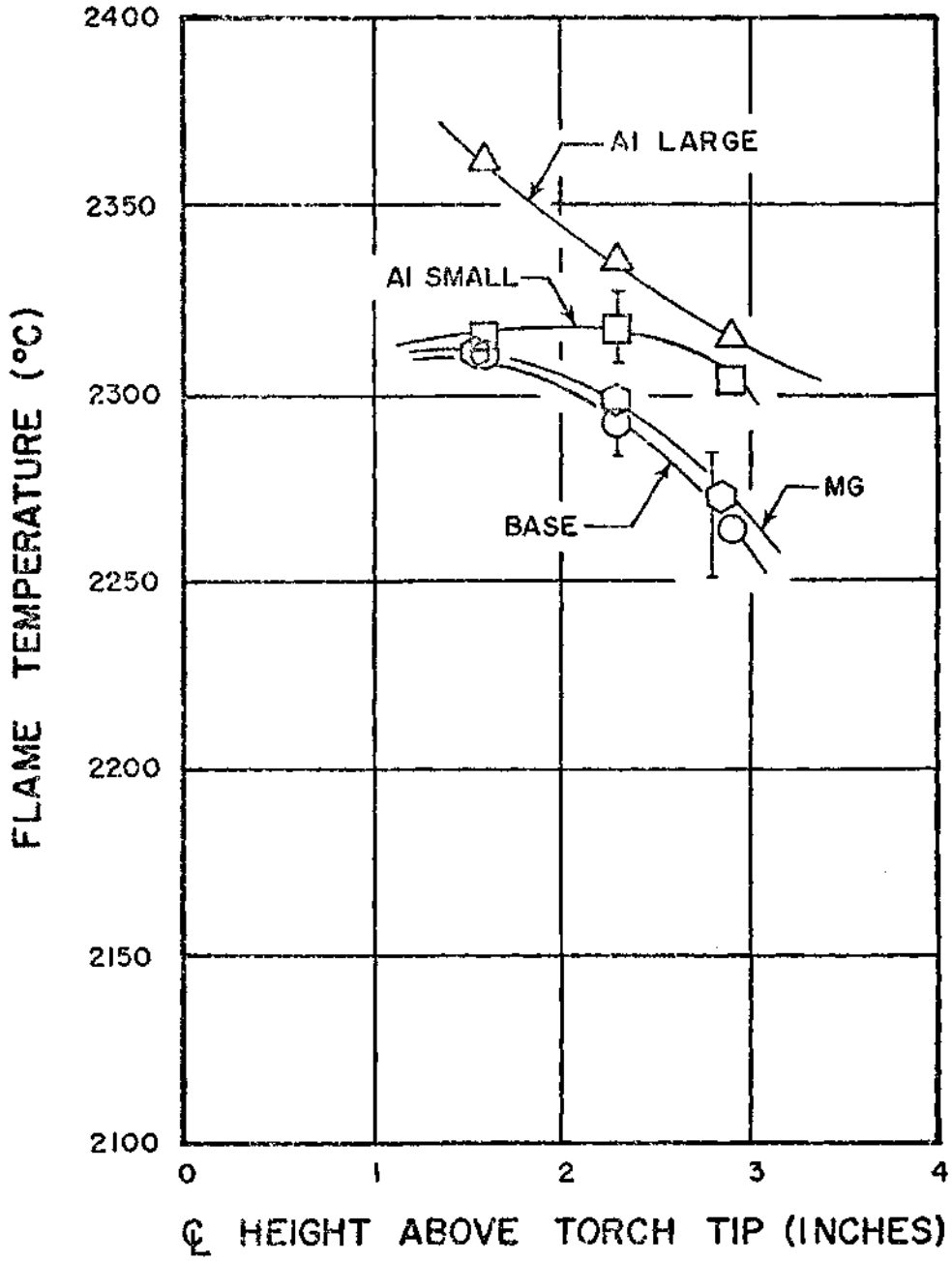

Figure 15. Temperatures of the Center Regions of Flame No. 4R.

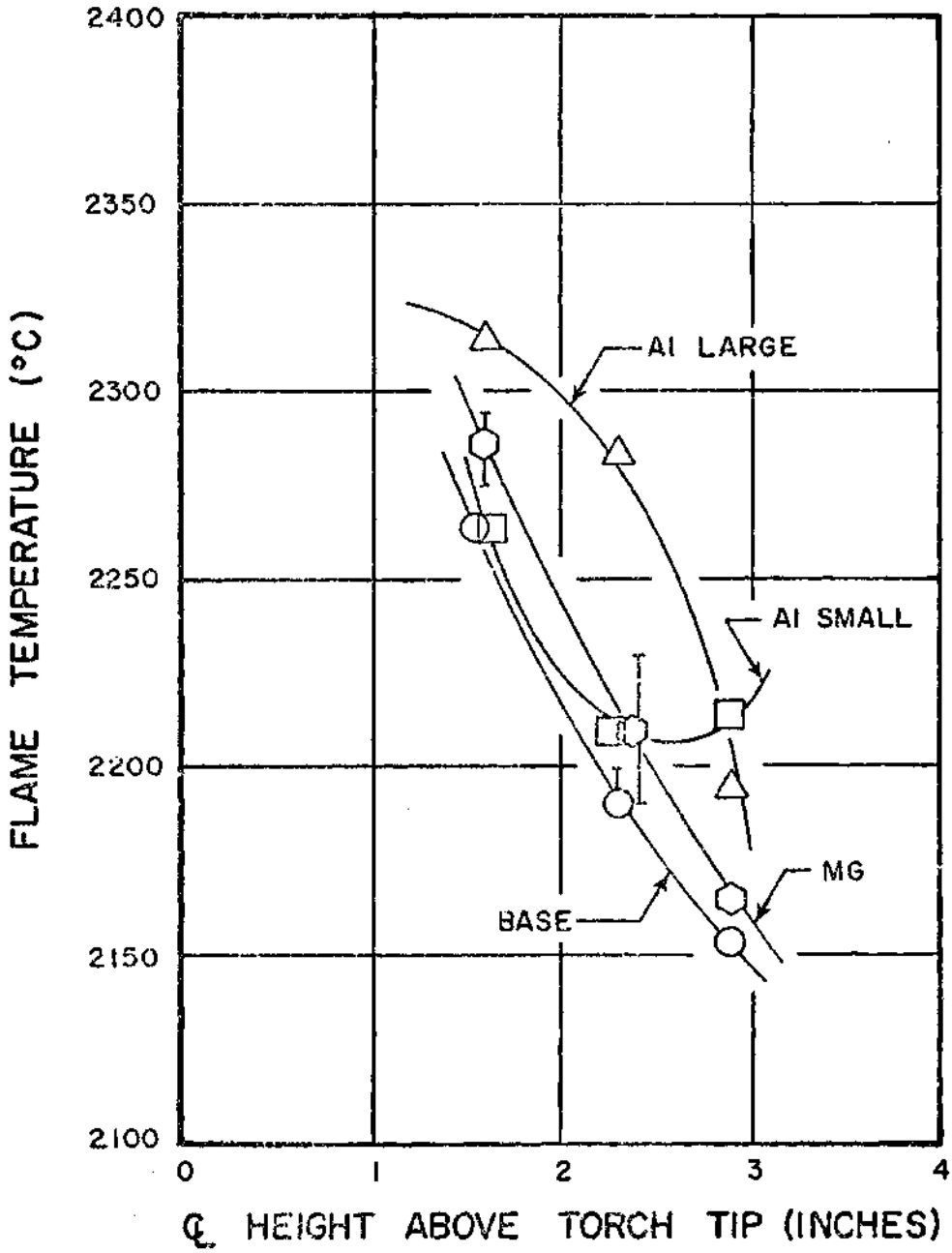

Figure 16. Temperatures of the Center Regions of Flame No. 2L.

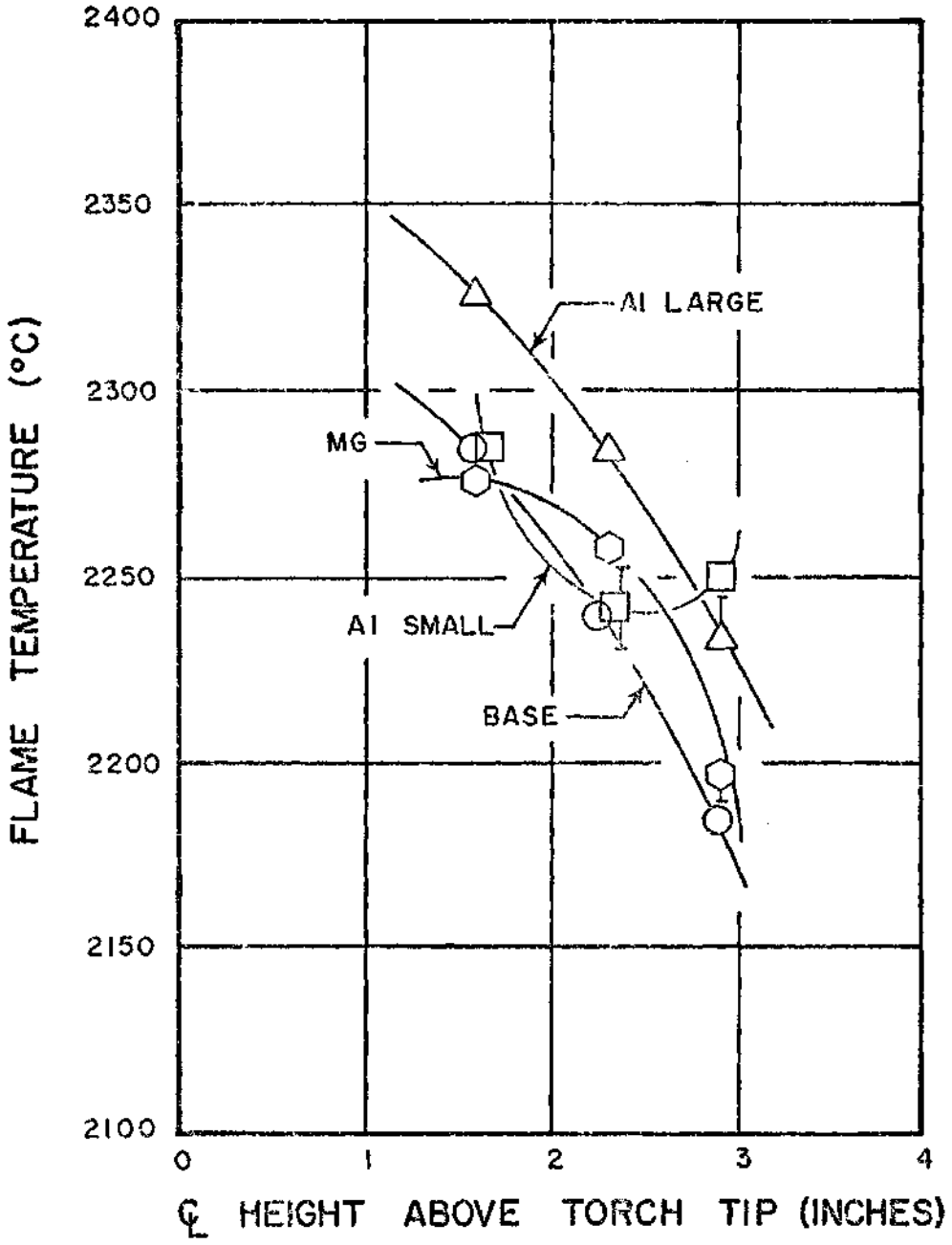

Figure 17. Temperatures of the Center Regions of Flame No. 3L.

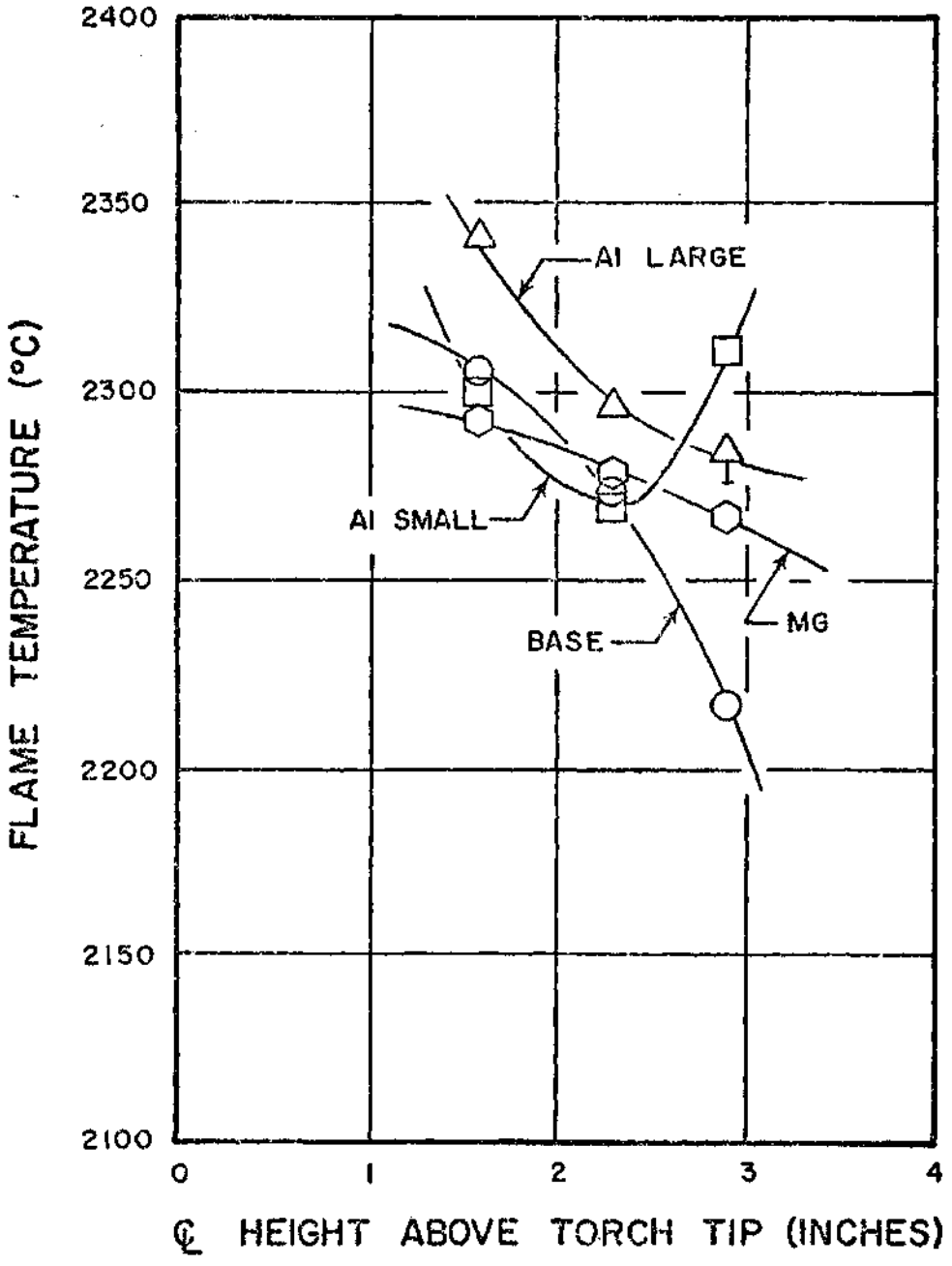

Figure 18. Temperatures of the Center Regions of Flame No. 4L.

A. Experimental Results

Figures 9 through 18 present the resultant data of this investigation. Each figure is a plot of the temperature of the centerline region of a flame against the height in the flame above the torch tip. It should be noted that although temperatures are plotted as points, the data taken is actually average temperatures of regions of the flame. In these figures average temperatures are plotted as points located at the centers of their corresponding regions. Four curves are drawn for each flame and are labelled "Base," "Al Large," "Al Small," or "Mg" indicating the presence in the flame of no metal particles, 35 micrometer aluminum particles, 19 micrometer aluminum particles, or magnesium particles, respectively.

Base Flame Temperature Effects

The flame mixtures listed in order of increasing base flame temperature are Nos. 2L, 1, 3L, 2, 2R, 4L, 3, 3R, 4R, 4, and 5. The temperature of the region nearest the inner cone of the flame varied from 2263°C, a 59°C difference. A range of 127°C was noted in the temperature of the uppermost region of the flames studied, from 2151°C to 2278°C.

Figure 19 plots the change in temperature of the flame due to the effects of the introduction of the metal powders against the base flame temperature.

The data points are widely scattered and no consistent trend is apparent. The increases in temperature due to the reaction of the metal powders may seem to decrease slightly with the increased flame temperatures, but these higher temperatures of the base flame were obtained

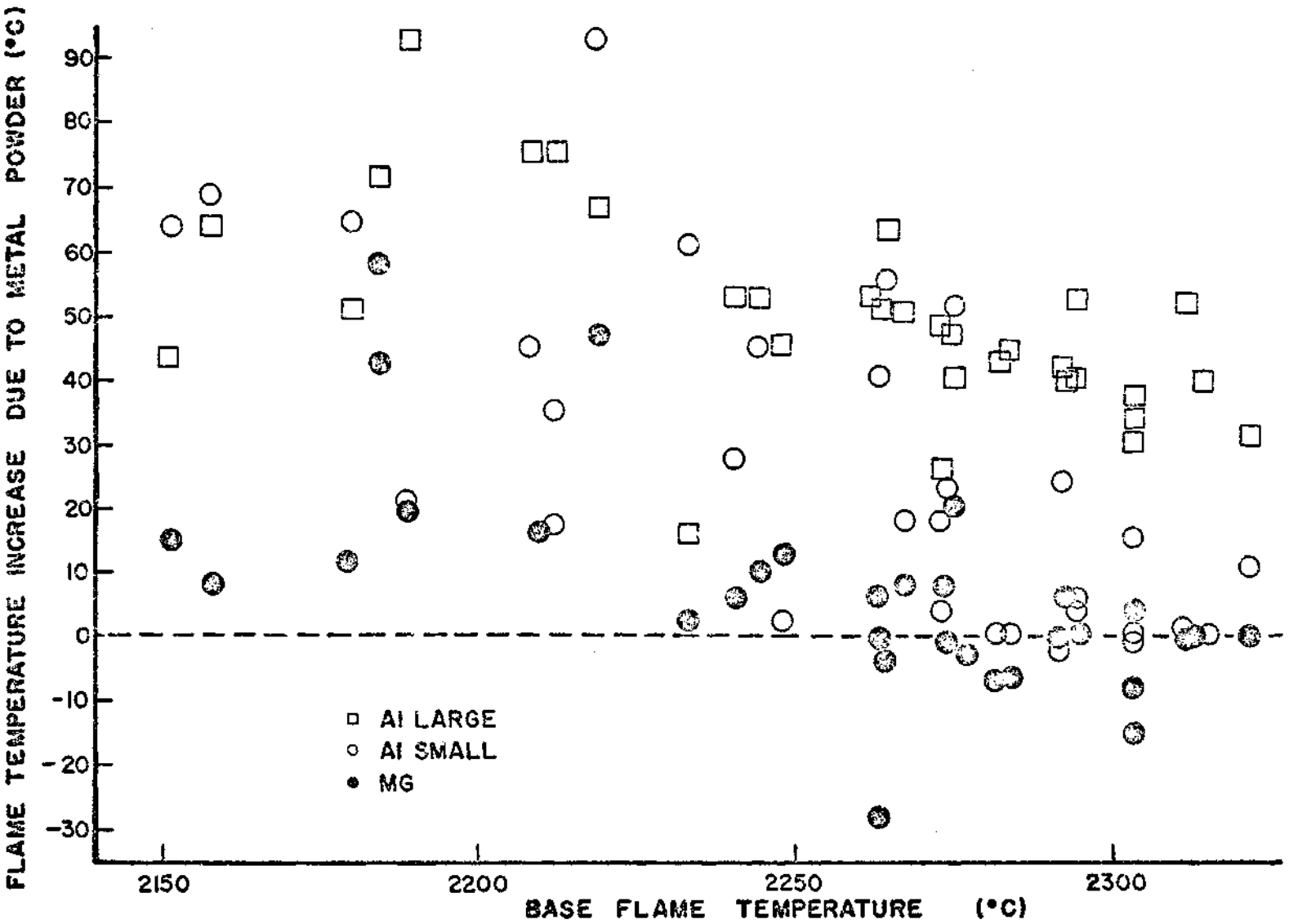

Figure 19. Flame Temperature Effects on Particle Reaction.

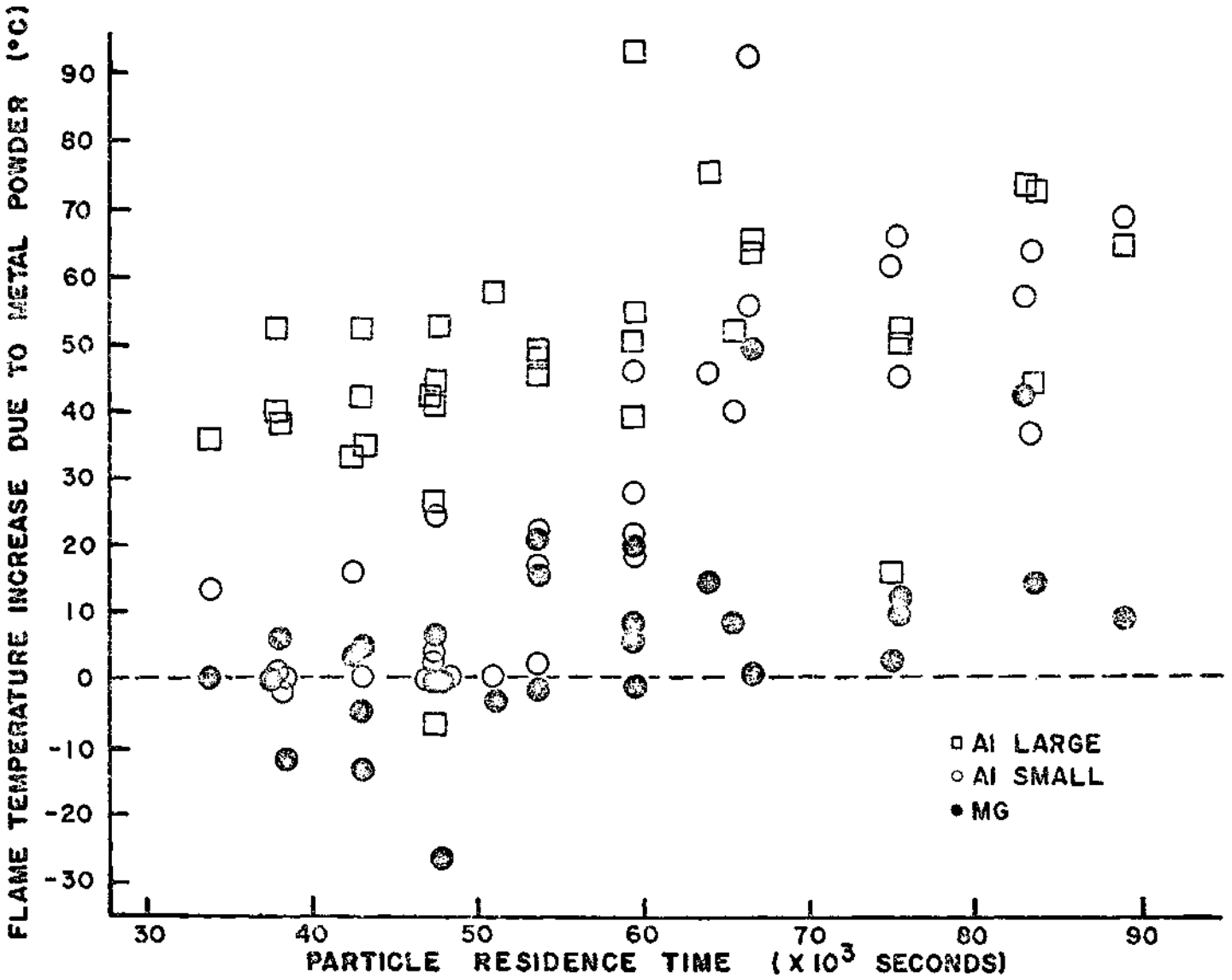

Figure 20. Residence Time Effects on Particle Reaction.

through increasing the volume flow rates of the reactants through the torch. The mass flow rates of the metal particles remained constant, however, and the dilution of this reactant species may account for this downward trend.

Particle Residence Time Effects

The increases in flame temperature as influenced by the particle residence time is illustrated in Figure 20. The data is again scattered but certain trends are evident. The increase in flame temperature due to the presence of the 19 micrometer aluminum particles and the magnesium particles moves from a zero or negative value to a positive increase as the residence time is extended. The 35 micrometer diameter aluminum particles exhibit similar behavior although for even very short residence times a substantial increase over the base flame temperature is noted.

Oxygen/Fuel Ratio Effects

In Figures 21-A, -B, and -C the effects of varying the o/f ratio are plotted. The abscissa of the coordinate systems in these charts is the increase in temperature of the average flame temperature with the particles present over the temperature of the average flame without the metal particles. The ordinate indicates the height above the torch tip of the region in the flame in which the temperature readings were taken.

For magnesium, Figure 21-A, in a stoichiometric flame mixture a slight decrease in temperature is noted at the lowest position in the flame and then the increase in temperature due to particle reaction increases steadily with height above the torch tip. In fuel rich

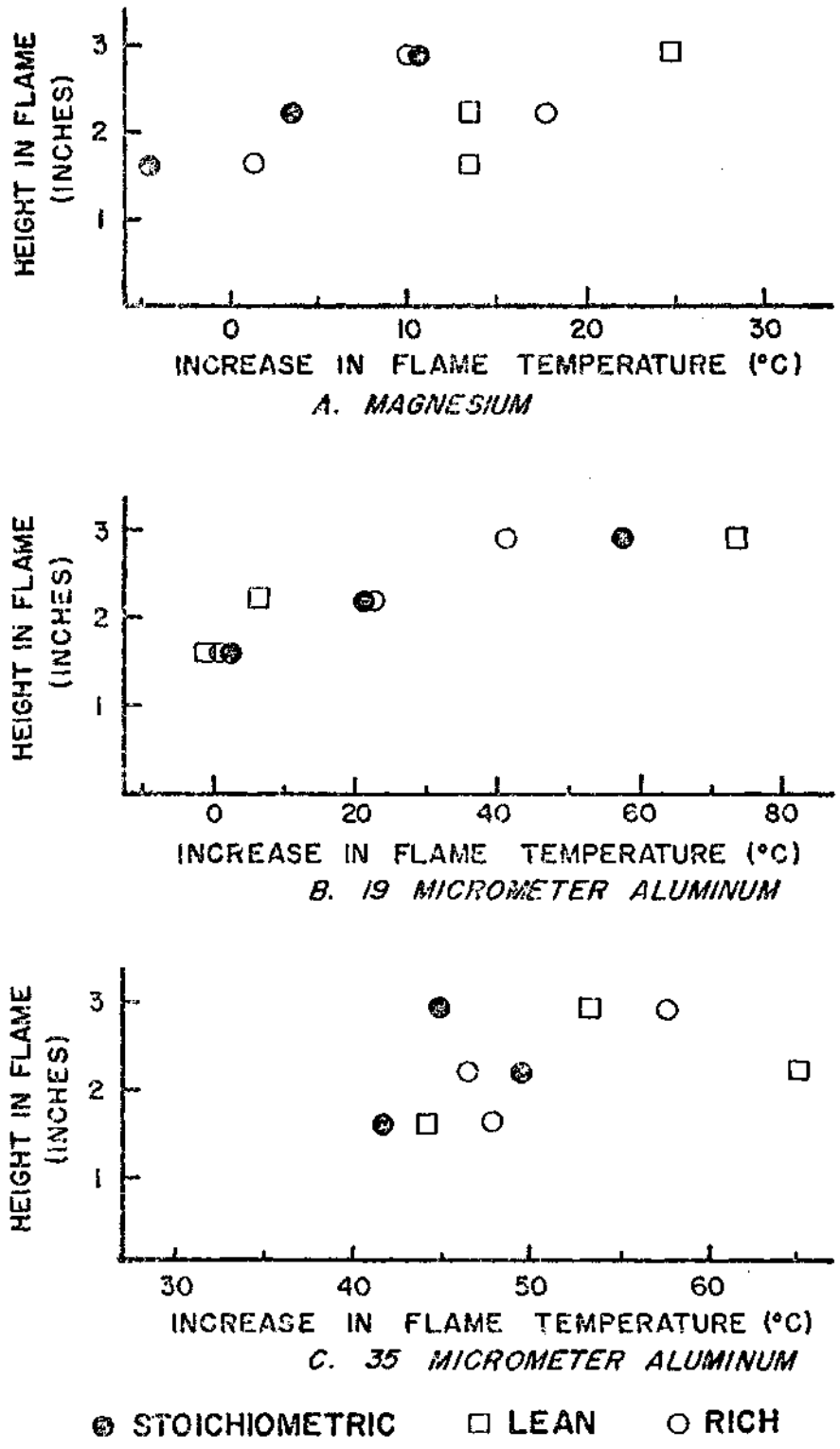

Figure 21. Oxygen Fuel Ratio Effects on Particle Reaction.

mixtures the increase in temperature is positive at the lowest region, reaches a maximum in the second region and then starts to fall off in the uppermost region. In lean flames a significant increase in temperature is noted at the lowest position of the flame studied. This value remains constant through the second region but then increases substantially at the highest region.

The 19 micrometer aluminum particles, Figure 21-B, seem to be affected least by a change in the o/f ratio. In lean, stoichiometric, and rich flame mixtures the introduction of these particles had little effect on the temperature measured at the lowest point in the flame. A slight increase was noted for the second region and a much larger increase was recorded in the highest region. Somewhat similar to the behavior of the magnesium, the aluminum particle reaction in lean flames did not lead to a substantial increase in the temperature difference between the first and second regions measured, but in the highest region the increase in temperature was greater for a lean mixture than for either stoichiometric or rich mixtures.

The 35 micrometer aluminum particles, Figure 21-C, exhibited perhaps the greatest change in behavior due to the o/f ratio. For the lean, stoichiometric, and rich mixtures a large increase in temperature was noted in the lowest region of the flame considered. But in the lean and stoichiometric mixtures the increase in temperature reached a maximum between the highest and lowest regions studied. The opposite was observed in rich mixtures; the increase in temperature dropped from that recorded in the lowest region and then increased to a higher value

as the third flame region is considered. The effect of varying the o/f ratio on the actual flame temperatures, not on the average temperature difference, with the introduction of these large aluminum particles is given in Figure 22, 23, and 24. In these charts the flame centerline temperatures for the flames with and without the aluminum particles for each of the o/f ratios are plotted.

B. Results Predicted by the Combustion Model

In this section, the metal particle combustion model as applied specifically to the magnesium and aluminum powders used in the investigation will be discussed. The anticipated effects of varying flame temperatures, o/f ratios, and particle residence times will be noted and correlated with the experimental results presented in the preceding section.

Magnesium

The temperature of the flame mixtures chosen in this investigation are above the boiling point of magnesium, 1381°K, but below the melting point of its oxide, 3075°K. Magnesium's Pilling and Bedworth ratio of 0.81 indicates the formation of a porous oxide shell. This oxide shell would not be formed if the particles were small, less than 20 micrometers in diameter, because heat transfer from the flame would quickly vaporize the magnesium and reaction would occur through a vapor phase diffusion flame some distance from the particle [5]. Solid MgO would be formed and dispersed as fine powder and no oxide shell would be formed. Combustion of the particles would be complete and very fast.

In this investigation, however, magnesium particles of 50 micro-

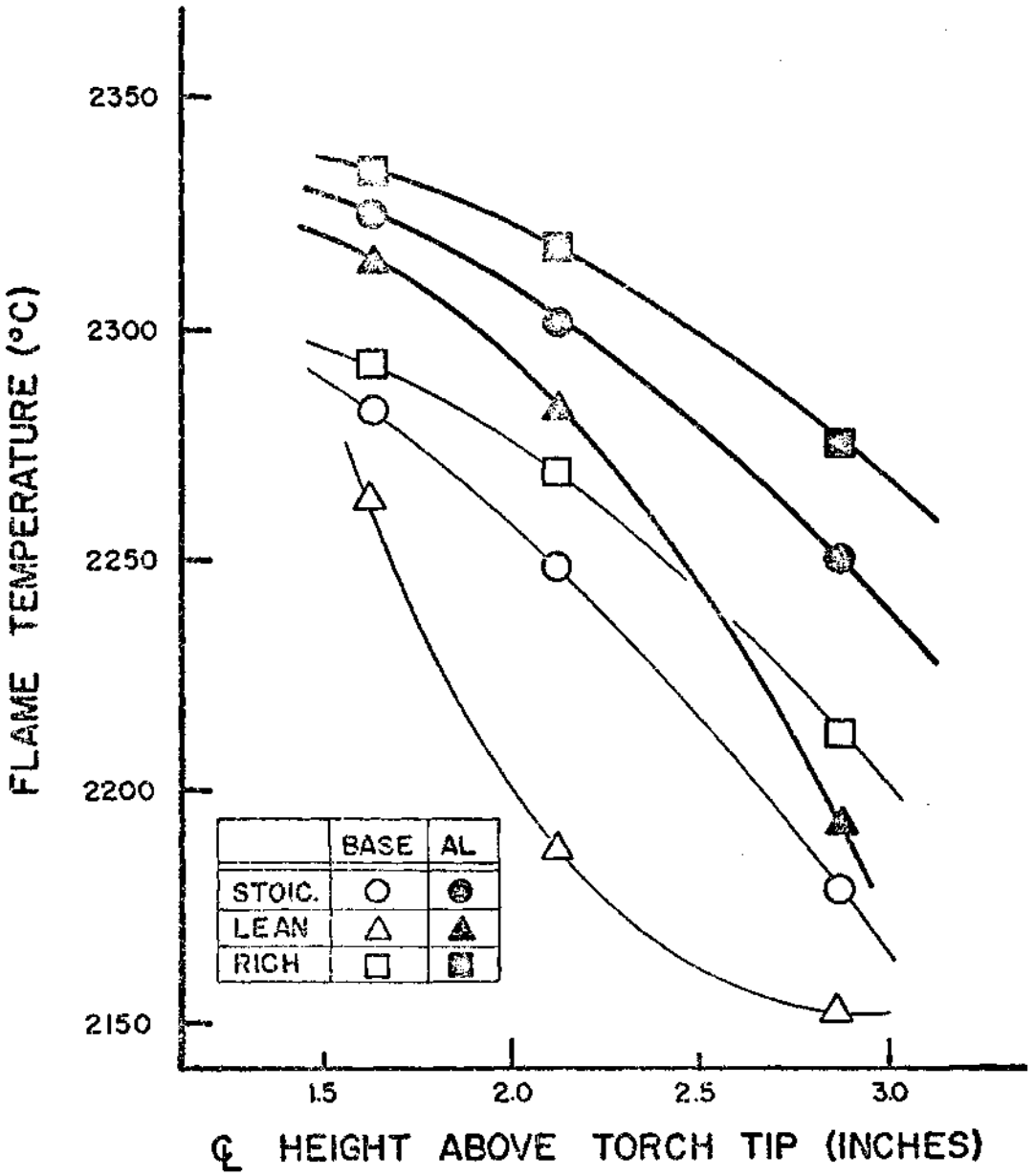

Figure 22. Effect of O/F Ratio (Flame Nos. 2R, 2, 2L).

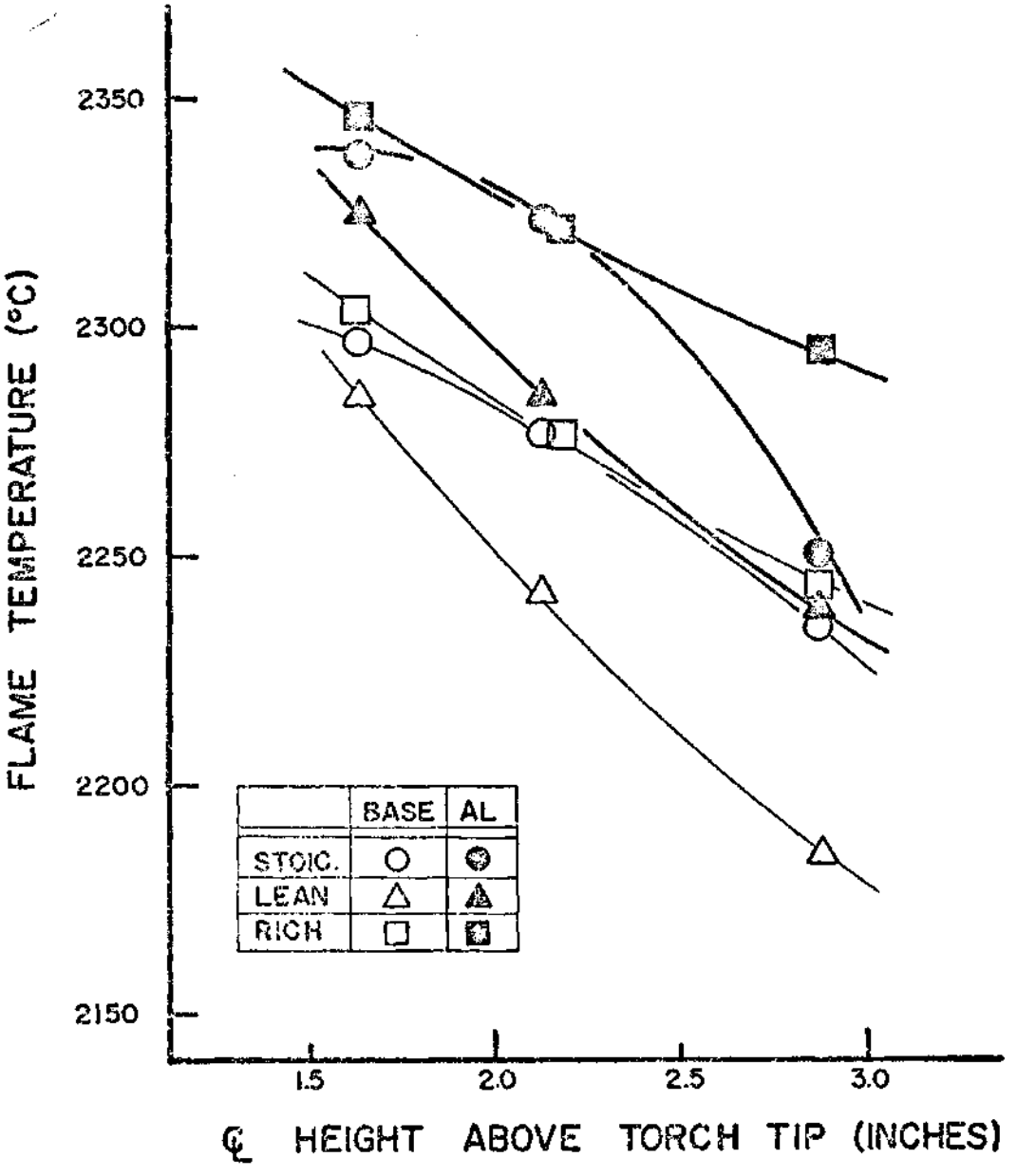

Figure 23. Effect of O/F Ratio (Flame Nos. 3R, 3, 3L).

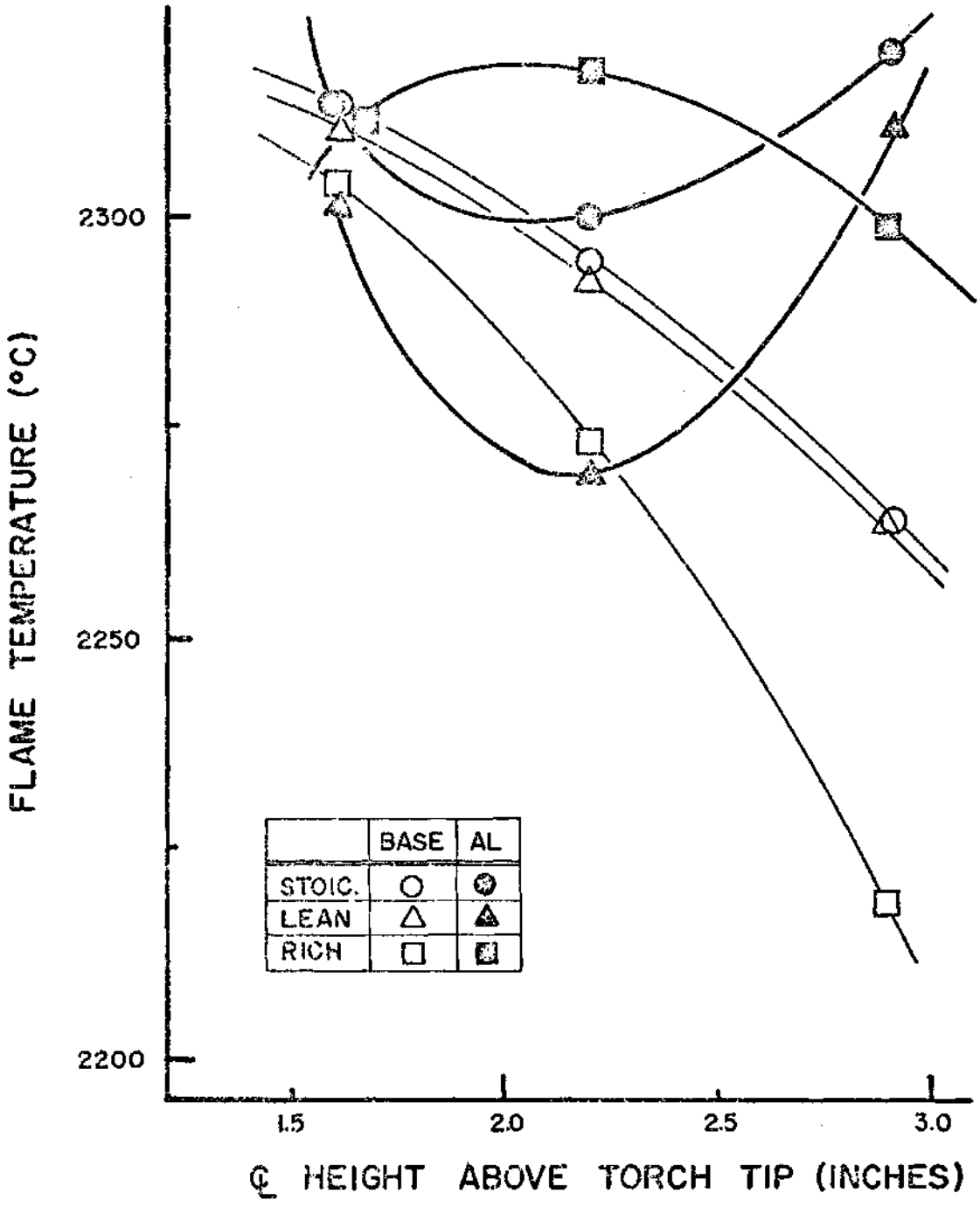

Figure 24. Effect of O/F Ratio (Flame Nos. 4R, 4, 4L).

meters in diameter were used. These large particles require longer residence times to reach the metal boiling temperature than the small particles discussed above. During this period of time significant surface oxidation occurs and a porous oxide layer is formed. Metal from the interior of the particle diffuses outward to react in a flame near the surface of the particle. The oxide layer continues to increase in thickness as the temperature of the particle rises. When the particle reaches the boiling temperature of the metal within its core, the particle may explode, bursting the oxide shell. This process of fragmentation may be observed as a sudden change in direction of the glowing particle within the flame.

Because the temperatures of the flames considered in this work all fall between the boiling point of the metal and the melting temperature of its oxide, no change in the reaction mode is expected for different base flame temperatures for the particle residence times studied. Fragmentation was observed in higher regions of several rich flames but this occurred far downstream of the regions of the flame this investigation is concerned with. This agrees with the results presented in the preceding section: no trend was apparent when the experimental data was examined to determine the possible effects of the base flame temperature.

Particle residence times should strongly affect the energy released in reaction. From the model proposed, one would expect immediate oxidation of the metal on the surface of the particle followed by a period of little reaction in which the particle is heated

to the melting point of the metal. Then a slow continuous reaction is expected while the particle is heated to the boiling point of the metal. Finally, fragmentation and a very rapid reaction would occur.

The data presented in Figure 20 of the previous section shows a gradual increase in the temperature of the flame with the magnesium particles present over the flame without the particles, as the residence time is extended. Isolated cases, Flame Nos. 2 and 4L, show a sharp rise in the temperature, but the general trend is from a zero or negative effect on the base flame temperature for short residence times increasing to a small positive effect for longer residence times.

The zero or negative effects for the shorter particle residence times could lead to the interpretation that the energy released by surface oxidation of the particles is at least balanced by the heat absorbed by the particles from the flame. The slow rate of energy release for longer residence times would seem to be indicative of a slow diffusion mode of combustion.

The influence of the oxygen/fuel ratio should be directly related to the particle residence time effects. A stoichiometric flame should result in a slow increase in the difference of the flame temperatures with and without the particles as the residence time is lengthened. For a lean mixture, one would expect the surface oxidation to occur earlier during the particle's residence in the flame followed by a period of little reaction as the particle is heated to the melting point of magnesium. Then, as diffusion of this liquid metal to the particle surface occurs, again reaction should take place, this time as a slow diffusion

flame at the surface of the particle. For fuel rich flame mixtures the surface oxidation and later diffusion burning should be retarded and occur at later stages in the particle residence times than was observed for the reaction in the lean mixtures.

Verification of this theory for the cases of stoichiometric and lean flames is indicated by the data presented in Figure 21-A. The results of the rich mixtures indicate a slight increase in energy released in the first region followed by a sharp rise by the time the particle has reached the second observed region. A decrease in temperature effect was recorded for the highest region. One explanation of this observed behavior could be that because surface oxidation had not been completed by the time the particle had entered the first region, loss of energy from the flame to the particle in melting the magnesium had not occurred to any great extent. The rise noted in the second region being dur to the continued surface oxidation mechanism, the drop recorded in the third region could be accounted for by the energy absorbed by the particle in melting its magnesium core.

Aluminum: 19 Micrometer Diameter Spheres

The temperature of the flames in this investigation fall in a range above aluminum's melting point, 932^{o}K, but below its boiling point, 2740^{o}K, and above the melting point of its oxide, 2318^{o}K. As was noted in Chapter I, aluminum with its Pilling and Bedworth ratio of 1.45 tends to form a sealing protective oxide layer.

In the temperature range of this investigation, the behavior of small aluminum particles is expected to be somewhat similar to the

behavior of the larger magnesium particles discussed earlier. Immediate oxidation of the aluminum at the surface of the particles is expected which would form an oxide layer shielding further reaction. But the temperature of the flames is hot enough to melt both the aluminum in the core and this oxide layer. Diffusion of aluminum outward through the molten oxide layer should result in a slow reaction at the particle's surface, further increasing the thickness of the oxide layer. Combustion in this manner should continue until all the aluminum in the particle had reacted. A sphere of liquid aluminum oxide would result.

As with the magnesium particles, this surface oxidation followed by a slow diffusion reaction are the only mechanisms of combustion expected to be found in the examination of flames containing these small aluminum particles for the temperature range studied. There then should be no significant trend apparent in studying the effect of the flame temperature on the reaction of these particles. The wide scattering of the experimental data of Figure 19 indicates at least negative confirmation of this prediction.

Because their modes of reaction are similar, the effects of particle residence times for the reactions of the magnesium particles and for the small aluminum particles should also be similar. As presented in Figure 20 a steady increase of particle reaction with residence time is noted for both powders. The greater temperature increases evinced by the aluminum particle reaction over the reaction of the magnesium particles could be accounted for by their higher mass flow rate, 1.61 and 0.162 grams per hour respectively.

As with the magnesium particles, the effect of the oxygen/fuel ratio should influence the time at which the different modes of reaction occur during the particle's residence in the flame. The speed with which surface oxidation occurs and the diffusion mode of reaction begins should be affected by the amount of oxygen accessible to the particles. The transition from surface oxidation to diffusion reaction should be accelerated in the lean mixtures and retarded in the rich mixtures.

The data present in Figure 21-B would seem to indicate that the surface reaction phenomena is predominant in both the rich and stoichiometric flame mixtures for the regions studied. The degree of reaction increases at almost a constant rate for these two mixtures with a slightly larger increase in temperature occurring in the stoichiometric flames than in the rich flames.

In the lean flames a study of the lowest region of the flame reveals little net energy release, followed by a slight energy release in the second region, and finally a substantial increase in the highest region. The small energy released in the first region could be accounted for by the heat released in surface oxidation being primarily returned to the particle in raising its temperature to the melting point of the oxide shell. Heat would continue to be absorbed by the particle as the second region was entered. Then, assuming that the oxide shell had melted, the large increase in temperature encountered in the third region could be accounted for by reaction in the diffusion flame mode.

Aluminum: 35 Micrometer Diameter Spheres

The combustion model for the smaller aluminum particles predicted

for the temperature range examined here two types of reaction: surface oxidation followed by a slow reaction by diffusion through the molten oxide layer.

For these large aluminum particles, however, heat transfer from the flame is not expected to be great enough during the particle residence times studied to cause the oxide layer to melt. Hence, the only reaction expected is the surface oxidation which would form a shielding layer preventing further reaction.

As with the other two powders, flame temperature variation over the range considered in this investigation should have little effect on the reaction behavior of the particles.

Energy released through surface oxidation should increase with particle residence times until the formation of the oxide layer is complete. Thereafter, further increasing the residence time should result in no additional reaction.

Figure 20 indicates a substantial reaction had already occurred previous to the particles' entering of the lowest region of study. This was evinced by a large increase in temperature for low particle residence times. As the residence time was increased, the data becomes more scattered, but a slight increase in the temperature difference between flames with and without the particles is apparent.

This would indicate most of the surface oxidation occurs before the particles enter the first region of the flame. This process of combustion apparently continues through all three regions of the flames examined.

The o/f ratio should affect the reaction by retarding the surface oxidation in rich flames and accelerating it in the lean flames. The data presented in Figure 21-C is not consistent with these predictions. Aluminum particle reaction in the stoichiometric and lean flame mixtures apparently reaches a peak during its travel through the regions of study and then tapers off. The reaction in the rich flames show an opposite trend. The temperature difference between flames with and without the particles reaches a minimum and then show a sharp increase with increasing particle residence time in these mixtures.

One explanation of the data presented in Figure 23 is that the surface reaction had not occurred to any great extent when the particles entered the first region. The large increase in temperature recorded could be due to the particles in the flame reflecting and scattering light from the reference source so that a portion of it does not reach the spectrograph. If this scattering loss occurs to any great extent, the lamp would necessarily have to be adjusted to a higher temperature to accomplish reversal even if the actual temperature of the flame had not changed. The increases in temperature recorded in lean and stoichiometric flames for the particle reaction could be due to the surface reaction, countered to some extent by the effects of the decrease in number of the aluminum particles in the solid angle of light from the reference source to the spectrograph. This decrease in density occurs because of the diffusion of the aluminum particles outward from the centerline region into a cloud within the flame. A decrease of aluminum particles in the optical path would result in less scattering and, hence, a lower temperature of the reference source would be required

for reversal. The anticipated behavior of the particles in a rich flame--reaction by a retarded surface oxidation process--combined with this effect of decreasing the number of aluminum particles in the cone of light could result in the lowering of the detected reversal temperature in the second region, as is illustrated in Figure 21-C.

The outward diffusion of the aluminum particles continues as they enter the third region of the flame. Consequently, the number of aluminum particles participating in the scattering phenomena is decreased still further. This could account for the drop in the temperature difference in the lean and stoichiometric flame mixtures in this highest region. Surface oxidation of the particles in the rich flames between the second and third regions could account for the increase in the temperature difference for the highest region in fuel rich flames.

If, in fact, the scattering phenomena does affect the measured reversal temperatures to the extent indicated by the data of the large diameter aluminum particles, the reason this source of error was not detected in examination of the behavior of the smaller aluminum particles or the magnesium powder could be their lower mass flow rates. The mass flow rate of the 35 micrometer aluminum particles is three times that of the 19 micrometer aluminum particles and thirty times that of the magnesium powder.

C. Evaluation of the Technique

The purpose of this investigation was to assemble a system capable of analyzing the reaction behavior of metal particles in flames. The effects of flame temperature, particle residence time, and oxygen fuel

ratio were to be examined.

Because the reference source is required to at least reach the flame temperature for reversal, a limitation was placed on the maximum flame temperature. It could not exceed the safe operating limit of the reference lamp, 2430°C. This upper limit and the stability limits of the burner restricted the flame temperature to a range in which the flame temperature should not, and experimentally did not affect the mode of combustion. Other than this negative verification of one of the criteria used in forming the combustion model, the effect of flame temperature on the ignition behavior of the particles was not obtained in this investigation.

Particle residence time effects were studied to some extent, but the transition of magnesium reaction from diffusion burning to vapor phase ignition, although visibly apparent in the higher regions of some flames, could not be observed in the regions of the flame studied.

The transition from surface oxidation to diffusion burning of the smaller diameter aluminum particles may have been observed, but further examination of higher regions of the flames would be required to verify this.

This data taken in examination of flames containing the larger diameter aluminum particles leaves open to question whether any reaction occurs at all. The extent to which the scattering of radiation from the reference source by these particles might affect the reversal temperature was not examined.

The effects of varying the oxygen fuel ratio, however, did prove

to be a valuable tool in interpreting the experimental results. The combined effects of particle residence time and o/f ratio variation provided a means of suggesting possible reaction modes for the 19 micrometer aluminum particles and for the magnesium powder. It was through examination of the oxygen fuel ratio effects that the question of scattering was considered.

In Appendix II, the accuracy of the temperature measurements is evaluated. The contributing factors to possible error are considered individually and their effect on the temperature readings was noted. A maximum error of 58°C was anticipated for a single temperature reading. This seems quite high in comparison with the significant temperature differences presented in the chapter. But a great part of this error is due to the calibration of the reference lamp and losses in the optical system. These deviations from the actual temperature will be constant for the temperatures recorded in this investigation. Because temperature differences rather than actual temperatures are of primary concern here, these errors cancel out. The only errors of significance are those introduced by the visual threshold bounding the reversal detection, 2°C, and those due to the level of confidence in reproducing flow rates and torch position. In Appendix II the effect of this second source of error was calculated for an extreme case and was found to result in an error of 13°C. This represents the largest possible error introduced by the level of confidence attainable considering the worst combination of flow adjustment errors. The anticipated experimental error in determining

temperature difference is then 15°C.

The error determination present above represents an analytical approach to error evaluation. Because each data point was measured on three separate occasions, each measurement yielding upper and lower limits of the reversal temperature, an examination of the raw data should reveal the actual precision to which the temperatures are measured. In considering deviations of the six readings for each point from the average value, a reproducibility of the temperature to within 4.2°C is noted from the data with a maximum deviation of 40°C. Only eight readings of the 792 recorded in this investigation showed deviations from the average as large as 20°C.

CHAPTER V

CONCLUSIONS AND RECOMMENDATIONS

The discussion of the experimental data presented in the preceding chapter indicates that modification of the system assembled in this investigation would be required to allow significant observation of the reaction behavior of metal powders. Three main areas of difficulty were encountered: (1) the observations of the particle reactions were made in a temperature range in which the base flame temperatures had no effect on the particle behavior; (2) the residence times studied were not of sufficient duration to confirm transition from one mode of reaction to another; and (3) the effect on the reversal temperature of scattering or reflection of the radiation from the reference lamp by the metal particles in the flame was not known.

In this chapter, possible solutions to the problems listed above will be presented. The difficulties associated with their implementation will also be considered.

A. The Temperature Range

The temperature range may be extended upward through the boiling point of aluminum, 2740^{o}K, by the use of an oxygen-acetylene base flame instead of oxygen and methane. Temperatures as high as 3400^{o}K can be obtained with oxy-acetylene combustion. This falls below the boiling point of aluminum oxide, 3800^{o}K, but for long residence times fragmenta-

tion and vapor phase ignition could occur.

The primary difficulty associated with raising the flame temperature lies in overheating not the burner but the reference light source. The tungsten strip lamp used in this investigation has a manufacturer's predicted life of 150 hours when operated at temperatures below 2000°C. If the temperature is raised to 2300°C the lamp's lifetime is shortened to about 20 minutes. Only a few seconds of operation before failure occurs is predicted for the lamp filament temperatures in excess of 2400°C. To study flames of higher temperatures, then, either a different type of reference source is required or another means of temperature measurement must be utilized.

A carbon arc lamp is a possible high temperature reference source. Coupled with filters of known transmissivity, a rotating sector could be used to modulate the effective temperature of the arc to achieve reversal.

The carbon arc used to calibrate the reference lamp (Appendix II) was examined as a possible reference source but was discarded. Faint D line emission from the arc caused by trace sodium impurities in the electrodes hindered precise discernment of the reversal condition. But high purity electrodes are available and the carbon arc without the D line emission would serve as an effective high temperature reference source.

W. Snelleman, working in the field of flame spectroscopy [15] has designed an optical system which allows reversal of high temperature flames with tungsten strip lamps similar to the one used in this investigation. Two rotating sectors set at different apertures are

used; one is placed between the reference lamp and the flame and the other between the flame and the aperture of the spectrograph. A photomultiplier tube with quick response characteristics is used in conjunction with a frequency selector. The output from the photomultiplier tube at the appropriate frequency is monitored. With this technique reversal can be obtained for flame temperatures far in excess of the temperature of the reference source.

B. Particle Residence Time

Residence times of greater duration than those indicated in Chapter IV could not be studied because of the interference of the optical bench of the spectrograph with the downward travel of the torch. This optical bench can be removed to allow study of higher regions of the flames, but another structure would have to be assembled to position of the optical system. Correct optical alignment is critical to the accuracy of the temperature measurements so a suitably precise and stable structure is necessitated.

C. The Effect of Particle Scattering

This source of error must be corrected for if meaningful observation of the reaction behavior of the metal particles is to occur. The extent to which particle scattering of the reference radiation affects the reversal temperature could be determined using Doty's photomultiplier tube system.

The technique would involve the alignment of the slit of a photomultiplier tube across a wavelength interval in which the flame

with or without the metal particles does not radiate. Ideally, this wavelength interval should be close to the D line emission of the sodium ions in the flame.

The flame does not emit radiation in this interval so it should not absorb energy in the interval either. Light of this wavelength from the reference source should be unaffected by passage through a flame containing no particles, and affected only by scattering or reflection in passing through a flame containing metal particles.

Different voltages across the reference source would be required to obtain the same output of the photomultiplier tube for passage of reference radiation through a flame with the particles and one without the particles. When applied to the calibration curve of the reference lamp this voltage difference should yield the effect of scattering on the reversal temperature.

APPENDIX I

TEMPERATURE AND LINE REVERSAL CONSIDERATIONS

Because temperature and its determination by the sodium D line reversal technique formed the backbone of this investigation, some discussion of this property and of the theory of line reversal is in order.

A. Temperature and Thermal Equilibrium in Flames

Classical thermodynamics defines temperature as a state variable which relates one thermodynamic system to other systems with which it is in thermal equilibrium. Temperature determination of a thermodynamic system is made by bringing a second system into thermal equilibrium with the first. Characteristic of the second system, the thermometer, is that certain of its easily measured state variables--pressure, volume, electrical resistance, etc.--have been calibrated with respect to the system's temperature.

Statistical thermodynamics relates temperature with the distribution of the component molecules or atoms of a system among the various energy levels accessible to them. Disregarding the effect of external fields, energy may be stored in a system as kinetic energy of the molecules or as energy internal to the molecules themselves--rotational, vibrational, or electronic--as the internal degrees of freedom of the system in question dictate.

Each of these modes of energy storage may be regarded as thermodynamic subsystems, essentially independent of one another, each possessing its own temperature. For example, the kinetic temperature, T_k, may be defined in terms of the mean kinetic energy of the molecules by the following formula:

$$\overline{K.E.} = \tfrac{1}{2} m \overline{V^2} = 3/2 \; K \; T_k$$

Similarly, temperatures for the internal degrees of freedom, T_j, may be defined by the Maxwell Boltzman distribution formula.

$$N_j = \frac{N_o \; g_j \; e^{- E_j/k \; T_j}}{\sum g_i \; e^{- E_i/k \; T_i}}$$

When a system is in complete thermal equilibrium, each of these subsystems have the same temperature and the temperature of the thermodynamic system may be determined by measuring any one of these temperatures. When the system is not in thermal equilibrium the subsystem temperatures are not all equal and the concept of a temperature for the system has not meaning.

From the standpoint of statistical mechanics, thermal equilibrium can be obtained only if for each process of energy transfer from one particle to another within the system there exists an exact reverse process. This implies that at thermal equilibrium the number of particles activated by each process must exactly equal the number deactivated by its reverse process. This is known as the principle of detailed balance.

This last consideration, coupled with the fact that the existence of temperature is contingent upon the condition of thermal equilibrium, leaves open to question whether or not it is proper to consider temperature within a flame. A flame is continuously losing energy to the surroundings in the form of radiation. The emission process is not balanced by its reverse process, absorption. Clearly the principle of detailed balance is not verified.

For a region in a premixed flame above the inner cone, Boiteux [16] considered analytically the various energy transfer processes on an order of magnitude basis of the collisions required to attain thermal equilibrium. His results indicate that thermal equilibrium is indeed attained. The rate of energy loss by emission is small compared to the energy transfer between the thermodynamic subsystems. Further verification of this result was supplied by Wolfhard and Gaydon [17] who determined analytically for certain premixed flames that although the radiation loss cannot be entirely neglected, it does not cause significant violation of the detailed balance principle.

Experimentally, a number of investigators [18, 19, 20, 21, 22] have verified within experimental error the equality of translational, rotational, vibrational, and electronic temperatures in the outer cone of premixed flames. However, this condition of thermal equilibrium does not hold for the inner cone of these flames. Here, where species are being created and energy is being released, there is not sufficient time for a Maxwell Boltzman distribution of the energy in any subsystem to occur. This implies not only that there is no reason to suppose that

the subsystem temperatures are all equal, but also that since these temperatures are defined for a distribution which is not obtained even the subsystem temperatures do not exist.

B. Sodium D Line Reversal

The investigators cited in the preceding section demonstrated the existence of thermal equilibrium in the outer cone of premixed flames. The sodium D line reversal technique determines the electronic excitation temperature of sodium ions in the flame. Because thermal equilibrium does prevail, this temperature may be regarded as the flame temperature.

A detailed theoretical proof of the validity of line reversal techniques when applied to simple flames may be found in almost any text dealing with radiation pyrometry. In this section a brief analytical verification of the line reversal method will be given. Symbols and nomenclature are similar to those used by Tourin [23].

A statement of Kirchhoff's law is needed for this proof. This is the relationship between the absorption and emission of spectral radiant energy by a thermal radiator.

$$\frac{N_a}{\alpha_a(\lambda,T)} = N^b(\lambda,T) \qquad (1)$$

In this equation the superscript b refers to a black body while the subscript a indicates any thermal radiator. This law states that the spectral radiance of a body at wavelength λ and temperature T divided by its spectral absorptance at the same wavelength and tempera-

ture is equal to the spectral radiance of a black body.

Considering now the emission detected by the spectrograph of the flame, subscript f, and the reference lamp, subscript 1, through the flame the following equation may be written.

$$N_{1f}\ (\lambda,\ T_1,\ T_f) = N_f\ (\lambda,\ T_f) + N_1\ (\lambda,\ T_1)\ [1 - \alpha_f\ (\lambda\ T_f)] \qquad (2)$$

The spectral radiance of the lamp-flame combination is equal to the spectral radiance of the flame plus the spectral radiance of the lamp minus that energy from the lamp that is absorbed by the flame.

For the reversal condition, the emission observed by the spectrograph is the same as that for the lamp alone.

$$N_{1f} = N_1(\lambda,\ T_1) \qquad (3)$$

Substituting equation 3 into equation 2 yields the following result.

$$\frac{N_f\ (\lambda,\ T_f)}{\alpha_f\ (\lambda,\ T_f)} = N_1\ (\lambda,\ T_1) \qquad (4)$$

From the statement of Kirchhoff's Law, equation 1, the left hand side of equation 4 can be seen to be the spectral emittance of a black body at the flame temperature.

$$N^b\ (\lambda,\ T_f) = N_1\ (\lambda,\ T_1) \qquad (5)$$

The reference lamp may be regarded as a black body radiator at the brightness temperature of the filament, T_b, rather than the true

temperature of the lamp, T_l. Equation 5 may then be written

$$N^b(\lambda, T_f) = N^b(\lambda, T_b) \tag{6}$$

and it follows that

$$T_f = T_b$$

For the reversal condition, the temperature of the flame is equal to the brightness temperature of the reference lamp.

C. Self Absorption and Line Contours

The analysis of the preceding section holds only for isothermal flames. If the region of the flame studied is not isothermal, the analysis of the temperature measured by reversal techniques becomes complex.

The major limitation of line reversal temperature determination is that temperature is not measured at a point. The image of the reference lamp formed in the flame is of significant size. Furthermore, all specied which lie within the solid angle of radiation received by the spectrograph along the entire length of the optical path from the reference lamp to the slit jaws at the aperture of the spectrograph can participate in the emission or absorption process. Although the D line radiation is affected significantly only by the high temperature sodium ions in the flame, these ions range from a relatively low temperature near the edges of the flame to a high temperature in the center of the flame. The D line emission from the flame is then from regions which

vary considerably in temperature.

To establish the meaning of temperatures measured by reversal of radiation from a non-isothermal flame, some background theory concerning line emission and intensity contour must be considered.

In Figure A1 curves are presented which represent the line emission from A, a high temperature region; B, a lower temperature region; and C, the result of radiation from a high temperature region passing through a lower temperature region.

Emission and absorption lines are not of zero width. The effects of natural broadening (linked to the Heisenberg uncertainty principle), Doppler broadening (a function of the velocity distribution of the emitting species), and collision broadening serve to give the line definite width and intensity contour. Curves A and B represent simple line emission from isothermal regions of different temperatures. Note that the emission line of curve A has not only a greater maximum intensity than that of curve B, but also that this line has a significantly high intensity across a greater wavelength interval than the line emitted by the cooler region. This is because the broadening effects listed above are more pronounced at higher temperatures.

For emission involving the transition of electrons from an excited state to the ground state, as is the case of sodium D line emission, the emission lines are identical to the absorption lines. Emission from a high temperature region in passing through a cooler region would be attenuated by absorption in the cooler region. Because the absorption line contour is the same as that of emission, the effects of the cooler

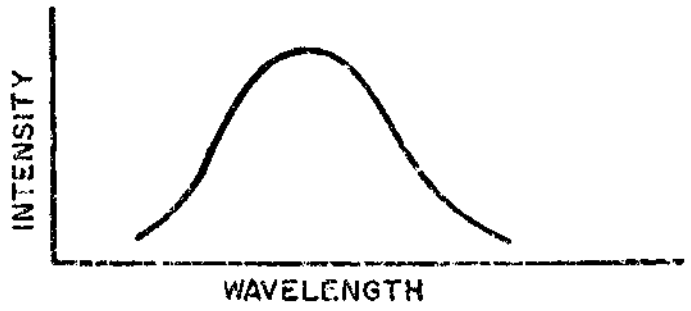

A. A HIGH TEMPERATURE REGION

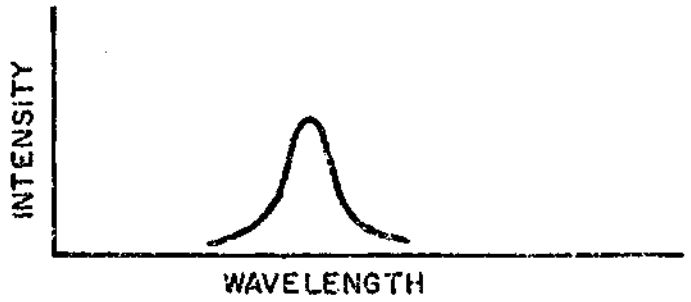

B. A LOWER TEMPERATURE REGION

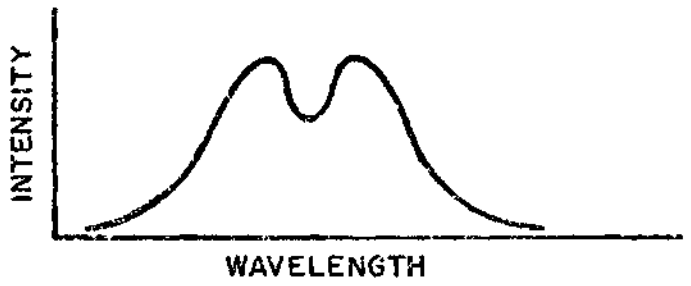

C. A HIGH TEMPERATURE REGION BEHIND A LOWER TEMPERATURE REGION

Figure A1. Intensity Contours of Line Emission.

region would be greatest at the center of the line and would trail off to zero as the distance from the center of the emission line is increased. An emission line of dimpled contour as illustrated by curve C would result.

When reversing this emission, the center of the line will reverse before the flanges. The value of the temperature recorded for reversal of this center region depends upon not only the temperatures of the two regions but also upon the number of emitting or absorbing particles in each of these regions.

The peaks in intensity at the outer flanges are very nearly unchanged by the self absorption process. Reversal of these peaks will yield a temperature which is very close to the temperature of the high temperature region.

All of the flames examined in this investigation exhibited self absorption to some extent. To minimize its effect the temperature recorded were those obtained by reversing the flange peaks of the D line emission.

The self absorption phenomena rendered the establishment of reversal temperatures more difficult, but with high resolution equipment the detailed examination of the D line emission dimpled by self reversal can provide a means of plotting temperature profiles within the flame (24). A second order dispersion from the diffraction grating scribed with 1200 lines per millimeter should provide the required resolution.

APPENDIX II

ERROR ANALYSIS

The causes of errors in the temperatures determined in this investigation may be divided into two areas: errors inherent to the line reversal technique, and errors introduced by the level of confidence in reproducing flow conditions and torch positions. In this appendix the effect of the contributing factors in each of these areas will be considered and a maximum deviation of the recorded temperature from the actual temperature will be ascertained.

A. Errors Inherent to the Reversal Technique

Sources of error inherent to the reversal technique include the precision with which the temperature of the reference source can be determined, losses in the optical system, and the threshholds of visual detection of the reversal condition.

The first source of error to be considered is the calibration of the reference source. The lamp used here was calibrated with a disappearing filament type optical pyrometer. Forsyth [23], choosing observers inexperienced in this type of work using a similar instrument demonstrated that an accuracy of $2^{o}K$ can be expected. However, the accuracy of this instrument is dependent upon the precision with which it is calibrated. Current to its platinum filament is adjusted manually and monitored by a galvanometer scaled to read temperature.

Doty [13] checked the calibration of this instrument using a Mole Richardson Type 2371 Pyrometric Molarc Lamp (carbon arc) equipped with filters as a reference source. He found the pyrometer's readings correct to within the accuracy of the filters, 35°K. Assuming the instrument's precision to be within one percent of the temperature measured, which is consistent with the above result, a calibration error of 27°K could be expected for the range of temperatures covered in this work.

Reflection errors are of two types: those occurring because of reflection by lens A (see Figure 6) of radiation from the reference source, and those caused by light from the flame being reflected by lens A, by the glass enclosure of the reference lamp, or by the lamp filament itself back through lens B and into the spectrograph. Both of these conditions would result in more radiation from the flame than from the reference lamp entering the spectrograph.

Reflection losses of the first type have been eliminated by calibration of the reference lamp through lens A. Snelleman [15], in analysing the second type of reflection losses determined that a temperature error of about 10°K was to be expected.

Stray light is considered to be radiation from any source outside the solid angle taken from the reference lamp to the aperture of the spectrograph. The main source of stray light is that portion of the flame not included in this solid angle. The effect of stray light was eliminated by the use of an aperture stop in the optical system.

The use of the high resolution spectrograph allowed a precision

of 2°K in visually detecting the reversal condition. This number was obtained by examination of the raw data taken in determining the upper and lower limits of the reversal condition. An average lamp voltage difference of 0.01 volts was noted bounding the reversal conditions. This voltage difference corresponds to the temperature error noted above.

B. Level of Confidence in Reproducing Conditions

Because each flame was constructed three times for each data point, the level of confidence in reproducing identical flow rates and torch positions introduces another source of error.

The accuracy to which the reactant gas flow could be controlled is 0.125 SCFH N_2, 0.05 SCFH O_2, and 0.01 SCFH CH_4. In applying these deviations in flow to Flame No. 2L in a combination which would lower the adiabatic flame temperature the most, a change in the adiabatic flame temperature of 21°K was noted. However, because of dissociation of the products and losses to the surroundings the actual temperatures noted in the flames were on the order of 65 percent of the adiabatic flame temperatures. Assuming this change of 21°K will be affected in the same manner to the same degree, an actual temperature error of 13°K should be expected.

A further source of error is now the precision with which the vertical height of the torch is adjusted. An estimated accuracy to 0.05 inches is expected. By examining the temperature plots of the flame centerline regions, Figures 8 through 18, this lack of precision could lead to a maximum error of 4°K.

C. Summary

Table 2 lists the errors contributed by each factor considered. As is indicated, an accuracy to 58°K is anticipated for the temperatures recorded in this work.

Table 2. Summary of Error Analysis

Source of Error	Magnitude
Calibration of the Reference Lamp	
Accuracy of the Pyrometer	27°K
Use of the Pyrometer	2°K
Reflection	
Losses from the Reference Lamp	0°K
Augmentation of Flame Radiation	10°K
Stray Light	0°K
Visual Detection of Reversal	2°K
Flow Settings	13°K
Torch Height	4°K
TOTAL	58°K

APPENDIX III

USE OF THE PHOTOMULTIPLIER TUBE

The application of the photomultiplier tube system constructed by Doty to line reversal temperature measurement will now be considered. Electronic monitoring of the reversal phenomena would not only avoid the severe eye fatigue encountered by this observer but should also lead to more consistent results. The problem of self reversal was noted in Appendix I. In this investigation the effect of self reversal was minimized by visually reversing the outer flanges of the reference lines, but a photomultiplier tube with its slit aligned over the resonance line emission could effectively integrate the intensity of radiation over the line width to determine the average value of the intensity of the radiation. A further advantage of the photomultiplier tubes would be that measurement of temperature profiles within the flame is possible through a method suggested by Strong and Bundy [24].

The first step in utilizing the photomultiplier tube system in line reversal work is the calibration of the output of the amplifier circuitry with the reference lamp temperature. The slit of the photomultiplier tube is positioned at a wavelength corresponding to one of the D lines. Then, with no flame and the reference lamp in its usual position the output of the photomultiplier tube versus the lamp voltage is plotted. This calibration is presented in Figure A2.

To measure the temperature of a flame seeded with sodium, the

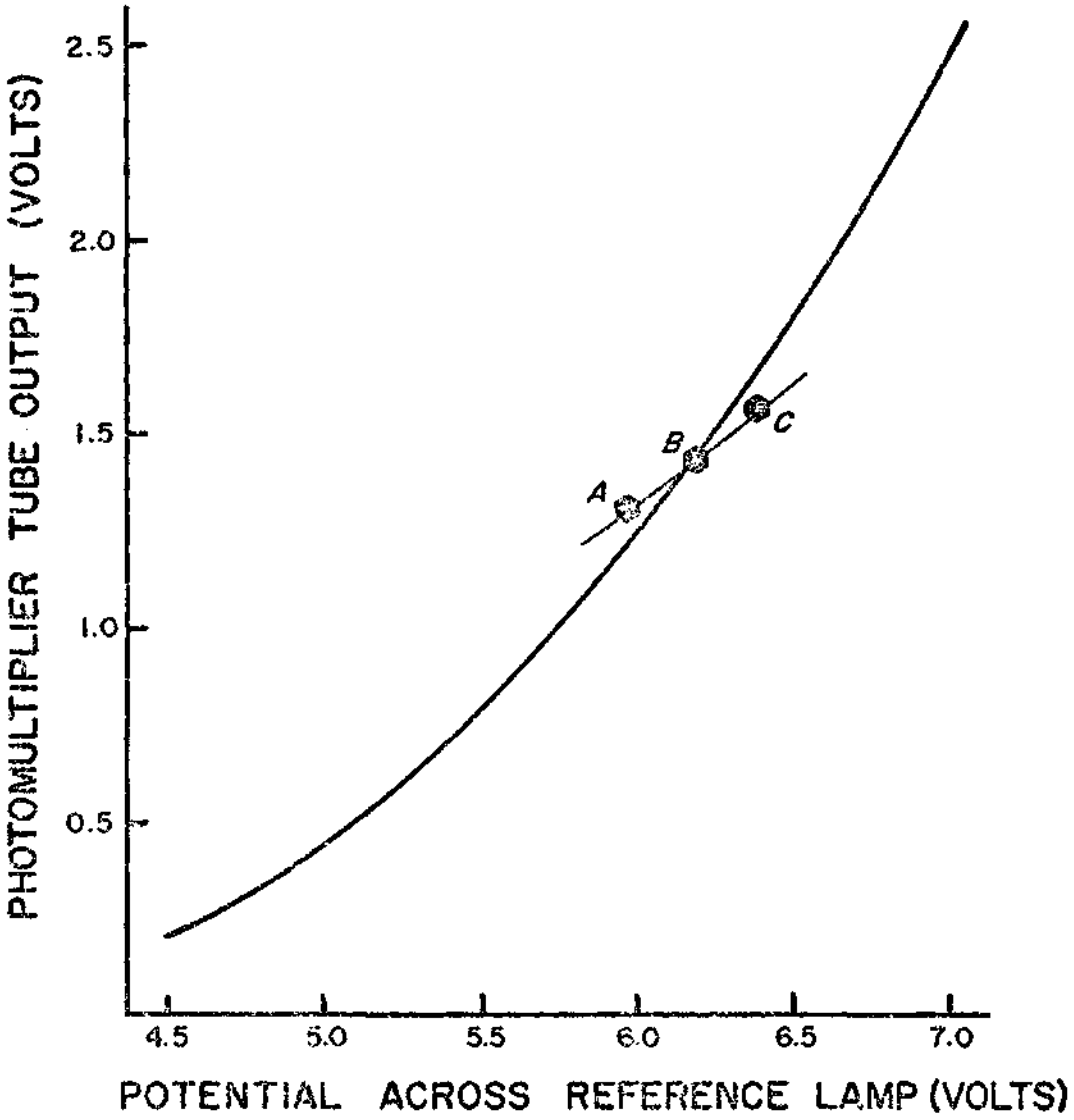

Figure A2. Photomultiplier Tube Calibration Curve.

reference lamp is set at several temperatures suspected to be near to that of the flame. The photomultiplier tube output for each of these reference lamp settings is plotted on the calibration curve of the lamp. These are shown as points A, B, and C on Figure A2. These outputs are representative of the energy emitted by the flame at that wavelength plus that emitted by the lamp minus that by the lamp which is absorbed by the flame. If the flame is at a higher temperature than the reference lamp, its emission is greater than its absorption and the data point will lie above the calibration curve for the lamp, point A. If the flame is at a lower temperature than the reference lamp, its emission is less than its absorption and the data point will lie below the calibration curve of the lamp, point C. The emission from the flame is exactly balanced by its absorption when the flame and the lamp are at the same temperature. The output in this case will lie directly on the calibration curve of the lamp, point C. The reference lamp temperature corresponding to this point of intersection is the reversal temperature, the temperature of the flame.

Use of an X-Y plotter was envisioned in this method of temperature measurement with the coordinate axes being the output of the photomultiplier tube amplifier circuitry and the voltage across the reference lamp. However, the extremely slow response of the amplifier, on the order of one minute, introduced excessive hysteresis and rendered this notion impractical. The presence of severe dark current drift in addition to the slow response of the system led to the discarding of photomultiplier tube monitoring in favor of visual observation of the reversal phenomena.

An attempt was made to determine the contour of the D line emission from flames in which self reversal was visually noted. The resonance line was scanned with the photomultiplier tube positioned by the micrometer gage attached to the photographic plate mount of the spectrograph. Contours similar to Figure A1-A were recorded, but no dimpled profile indicative of self absorption was obtained.

APPENDIX IV

SAMPLE CALCULATIONS

This appendix deals with three calculations for Flame No. 2L. The first calculation involves the determination of the correct flowmeter settings to produce the desired reactant mixture. The second is the calculation of this flame's adiabatic flame temperature. The third section of this appendix will present the calculation of the adiabatic flame temperature of this flame for maximum errors in flow adjustment. The difference in the adiabatic flame temperatures calculated in these last two sections is the temperature error caused by improper flow setting considered in the error analysis of Appendix II.

A. Determination of Flowmeter Settings

For the Flame No. 2L the desired flows of the reactant gases are 3.31 SCFH methane, 7.94 SCFH oxygen, and 4.75 SCFH nitrogen.

The ambient temperature and pressure are 77^{o}F and 28.87 inches of mercury, respectively.

The flowmeter calibration curves presented in Appendix V are for the flow of air at 70^{o}F and at 14.7 psia. Adaptation of these curves for use with the reactant gases involves correction for the molecular weights of the species and for their flow temperatures and pressures.

Neglecting these corrections for the moment, the flowmeter are adjusted to the settings indicated by their calibration curves which would

yield the correct flow rates. The following information is noted.

REACTANT FLOW	FLOWMETER SETTING	MANOMETER PRESSURE	TEMPERATURE
Nitrogen	20 mm	1.0 inches Hg	76°F
Oxygen	7.9 SCFH*	12.3 inches H_2O	77°F
Methane	86 mm	7.0 inches H_2O	76°F

The flow pressures and temperatures recorded above now allow correction for each of the reactant species. For variable area flowmeters of the type in use here, the following correction applies [26].

$$\dot{V}_b = \dot{V}_a \left[\left(\frac{x_a}{x_b}\right) \left(\frac{T_b}{T_a}\right) \left(\frac{P_a}{P_b}\right) \right]^{\frac{1}{2}}$$

The subscript a indicates the flow conditions for which the meter is calibrated; flow conditions encountered at the time of operation are indicated by the subscript b. Evaluating the term in brackets for the flow of each species, one finds

$$\dot{V}_{N_2} = 0.950\ \dot{V}_a \ ; \ \dot{V}_{O_2} = 1.005\ \dot{V}_a \ ; \ \dot{V}_{CH_4} = 1.351\ \dot{V}_a$$

The terms on the left hand side of the above equations are known. It remains to compute the flows on the right hand side.

$$\dot{V}_{aN_2} = \frac{4.75}{.950} = 5.00 \text{ SCFH}$$

$$\dot{V}_{aO_2} = \frac{7.94}{1.005} = 7.9 \text{ SCFH}$$

$$\dot{V}_{aCN_4} = \frac{3.31}{1.351} = 2.45 \text{ SCFH}$$

---

* The oxygen flowmeter is scaled to read directly in SCFH of air.

The flowmeters are adjusted to the new settings indicated by the results above.

REACTANT FLOW	FLOWMETER SETTING
Nitrogen	21 mm
Oxygen	7.9 SCFH
Methane	62 mm

Manometer pressures were found to change very little with these new flow settings. An analysis of the magnitude of the effect of the pressure change on the flow rate revealed that it was smaller than the precision to which the flow could be controlled.

B. Adiabatic Flame Temperatures

In the calculations here and in the following section reactions are assumed to proceed to completion. No dissociation effects were considered so a maximum value of the adiabatic flame temperature is computed.

A species balance for a lean flame mixture is presented below.

$$x\ CH_4 + y\ O_2 + z\ N_2 \rightarrow x\ CO_2 + 2x\ H_2O + (y - 2x)\ O_2 + z\ N_2 \qquad (1)$$

In the above equation, x, y, and z are the molar flow rates of the reactant gases. From this equation an energy balance for the reaction occurring at $77^{\circ}F$ may be written.

$$x\ (h_{CH_4} + h^{\circ}_{f\ CH_4}) + y\ h_{O_2} + z\ h_{N_2} = x\ (h_{CO_2} + h^{\circ}_{f\ CO_2})$$

$$+ 2x\ (h_{H_2O} + h^{\circ}_{f\ H_2O}) + (y - 2x)\ h_{O_2} - z\ h_{N_2} + 0 \qquad (2)$$

Q is the energy released in the reaction. Solving for Q,

$$Q = x\,[h_{CH_4} - 2h_{O_2} - h_{CO_2} - 2h_{H_2O} - h^{\circ}_{f\ CO_2} - 2h^{\circ}_{f\ H_2O}] \qquad (3)$$

Now substituting the values of the enthalpies and enthalpies of formation into the above equation yields

$$Q = 3.444 \times 10^5 \times \quad [BTU/hr] \qquad (4)$$

The energy released, Q, is used to raise the products from 77°F to the adiabatic flame temperature.

$$Q = x\,(h_{T\ CO_2} - h_{77^{\circ}\ CO_2}) + 2x\,(h_{T\ H_2O} - h_{77^{\circ}\ H_2O})$$

$$+ (y - 2x)\,(h_{T\ O_2} - h_{77^{\circ}\ O_2}) + z\,(h_{T\ N_2} - h_{77^{\circ}\ N_2})$$

or

$$3.444 \times 10^5 = h_{T\ CO_2} + 2h_{T\ H_2O} + (y/x - 2)\,h_{T\ O_2} + z/x\,h_{T\ N_2} - h_{77^{\circ}CO_2}$$

$$- 2h_{77^{\circ}\ H_2O} - (y/x - 2)\,h_{77^{\circ}O_2} - z/x\,h_{77^{\circ}\ N_2}$$

The energy balance presented above holds for the lean mixture flames considered in this investigation. Substituting in the flow coefficients, this equation may be solved by trial and error. The final result is

$$T_{adiabatic} = 6968^{\circ}F = \underline{3871^{\circ}K}$$

C. Errors Introduced by Inaccurate Flow Control

The adiabatic temperature of Flame No. 2L with the reactant flows improperly regulated is now considered. The maximum deviations from correct flow adjustment were determined to be 0.125 SCFH nitrogen, 0.05 SCFH oxygen, and 0.01 SCFH methane. These deviations are applied to the flow rates of Flame No. 2L in a combination which would have the greatest effect on the adiabatic flame temperature. Thus, the methane flow was decreased while the oxygen and nitrogen flows were increased, all by their corresponding maximum flow deviations.

REACTANT	CORRECT FLOW	ADJUSTED FLOW
Nitrogen	4.75 SCFH	4.88 SCFH
Oxygen	7.94 SCFH	7.99 SCFH
Methane	3.31 SCFH	3.30 SCFH

Substitution of these new flow rates into Equation 6 of the previous section and again solution by trial and error yields the adiabatic flame temperature of this improperly regulated flame.

$$T_{adiabatic} = 6924^{\circ}R = \underline{3850^{\circ}K}$$

The error introduced by imprecise flow control of the reactants is the difference between this adiabatic flame temperature and the one computed in the previous section: $21^{\circ}K$.

APPENDIX V

PARTICLE SIZE DISTRIBUTIONS, FLOWMETER AND REFERENCE LAMP CALIBRATION CURVES

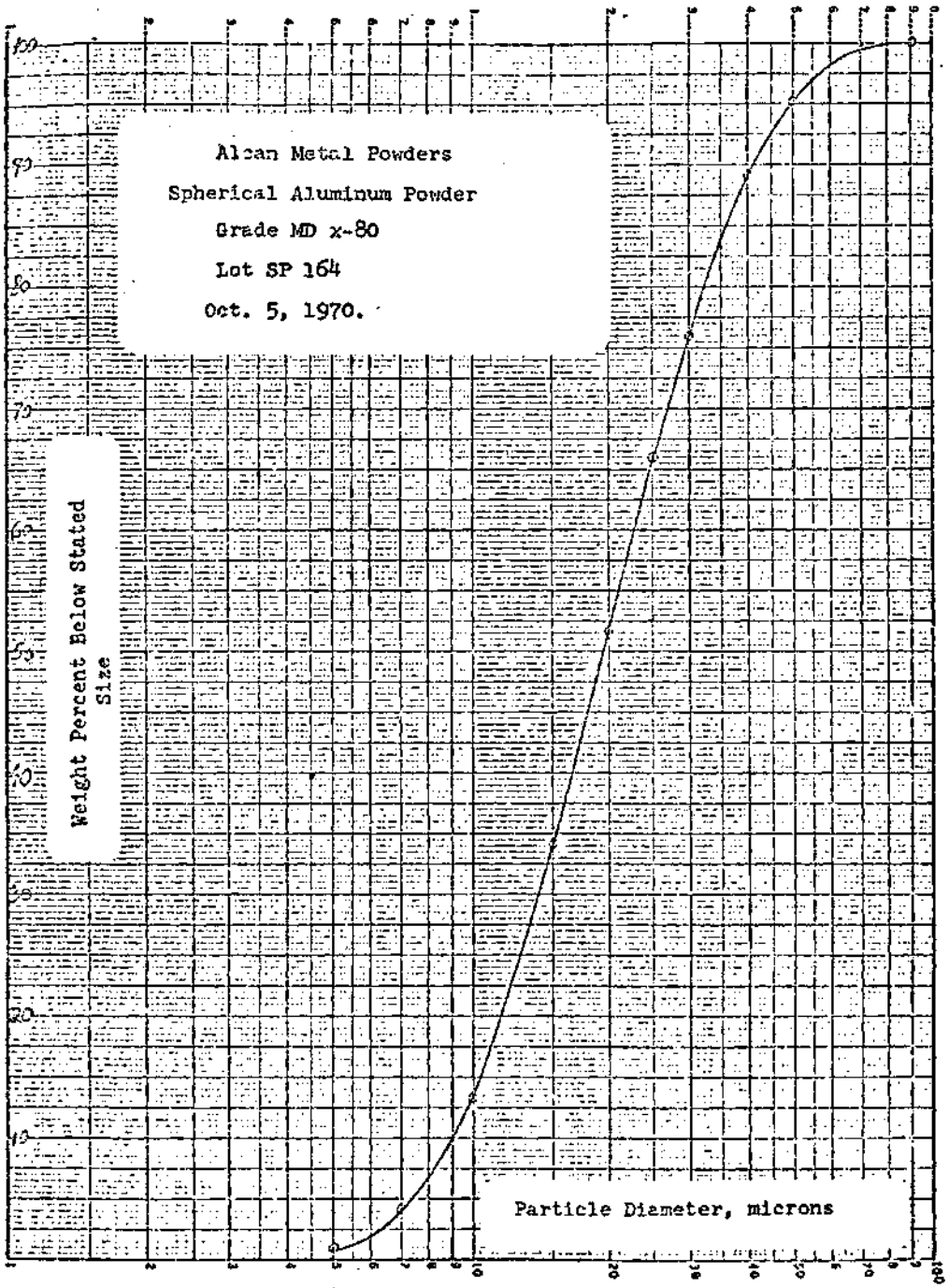

Figure A3. Particle Size Distribution within the 19 Micrometer Diameter Aluminum Powder

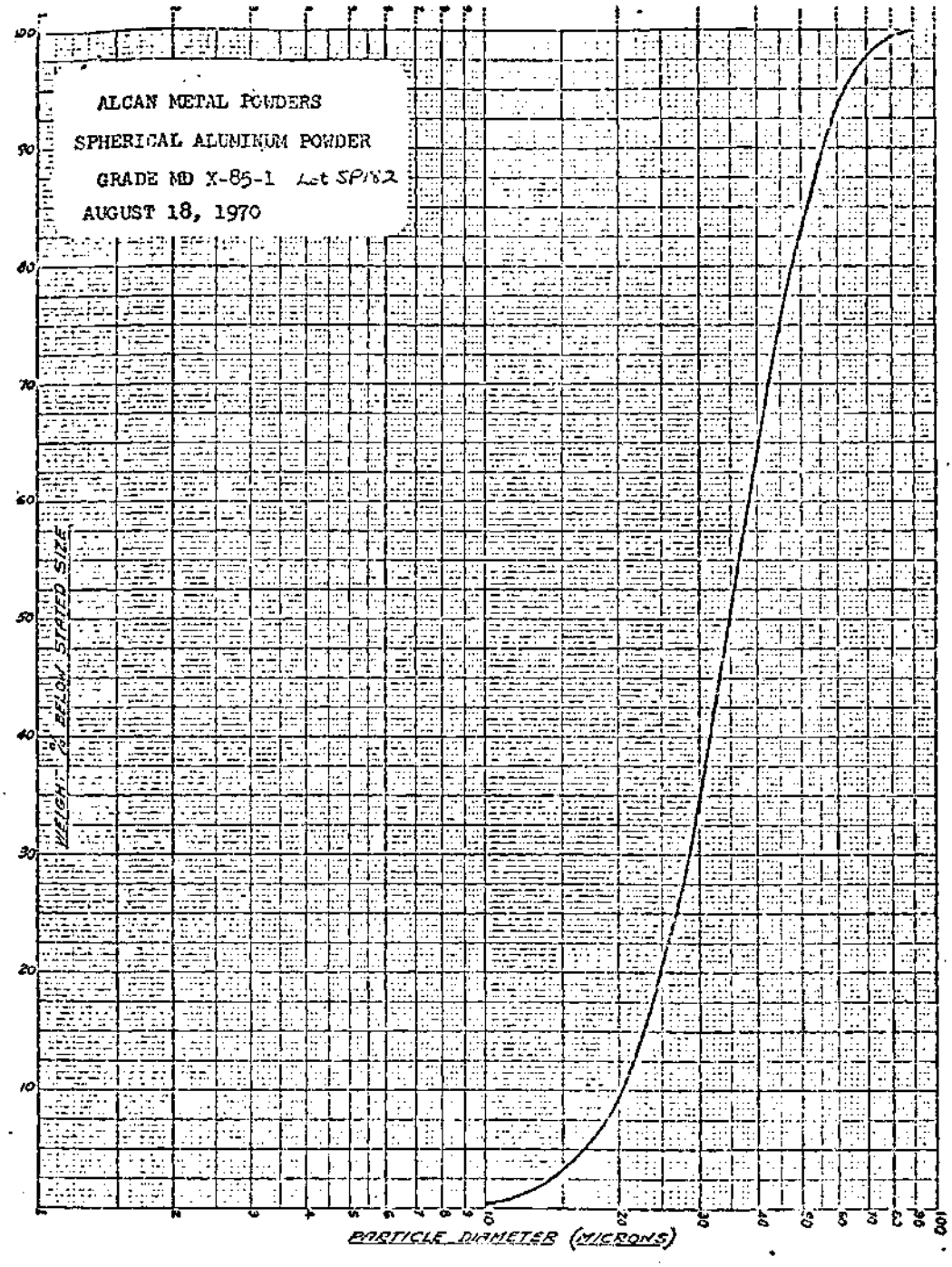

Figure A4. Particle Size Distribution within the 35 Micrometer Diameter Aluminum Powder

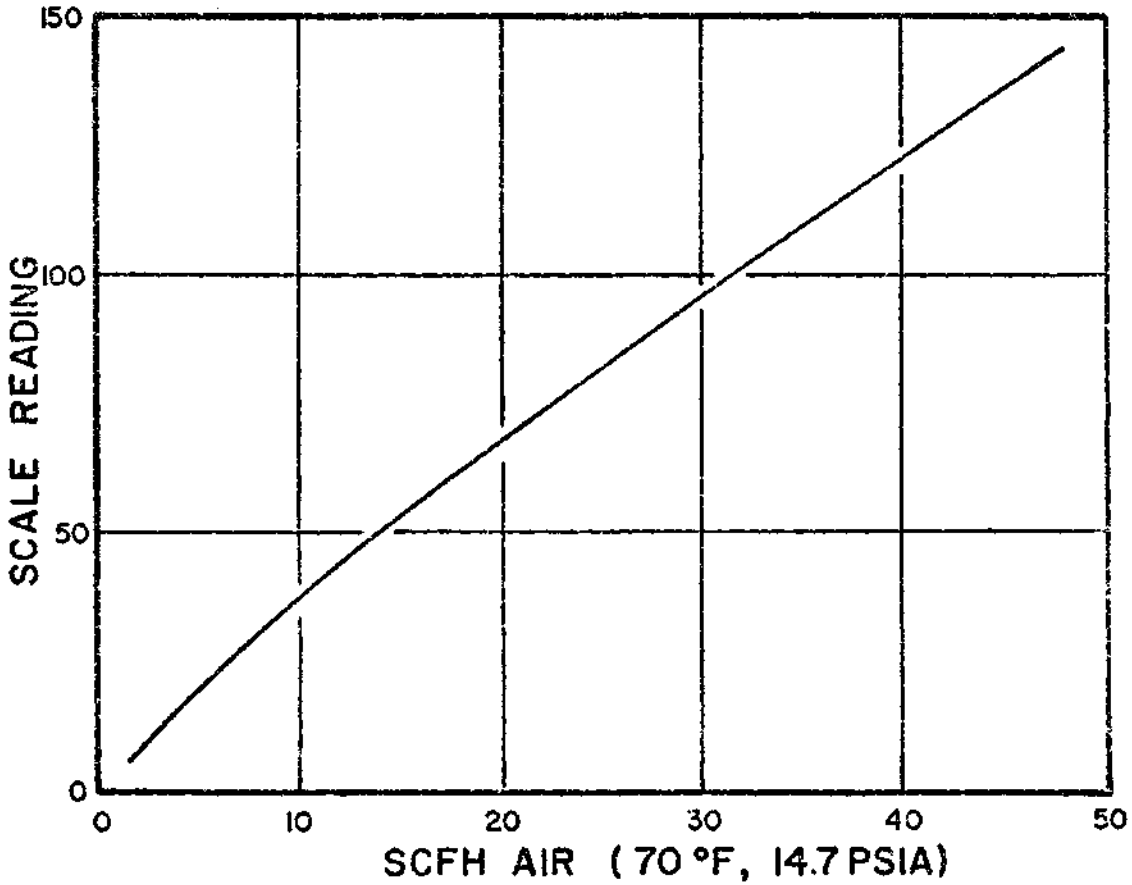

Figure A5. Nitrogen Flowmeter Calibration Curve

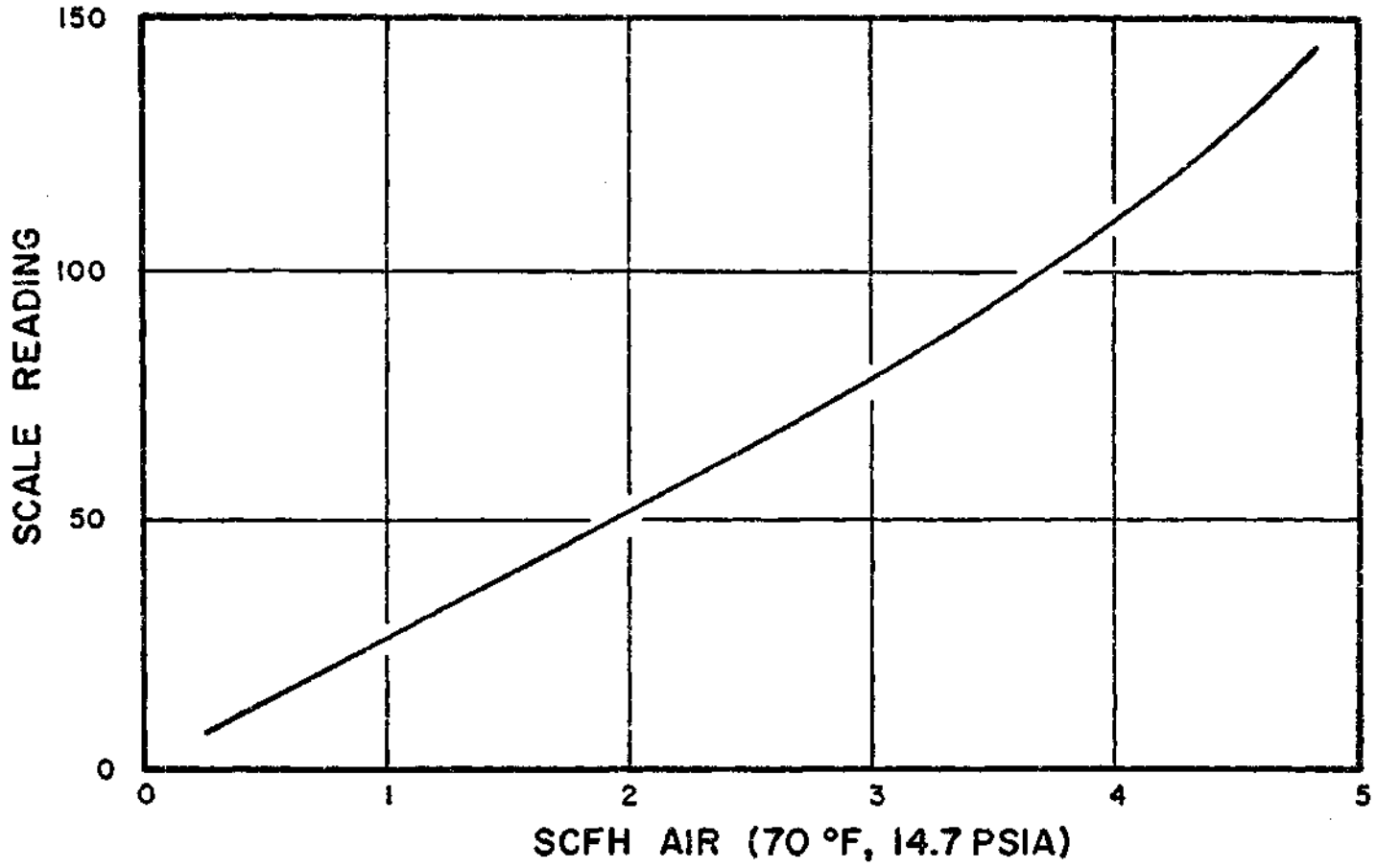

Figure A6. Methane Flowmeter Calibration Curve

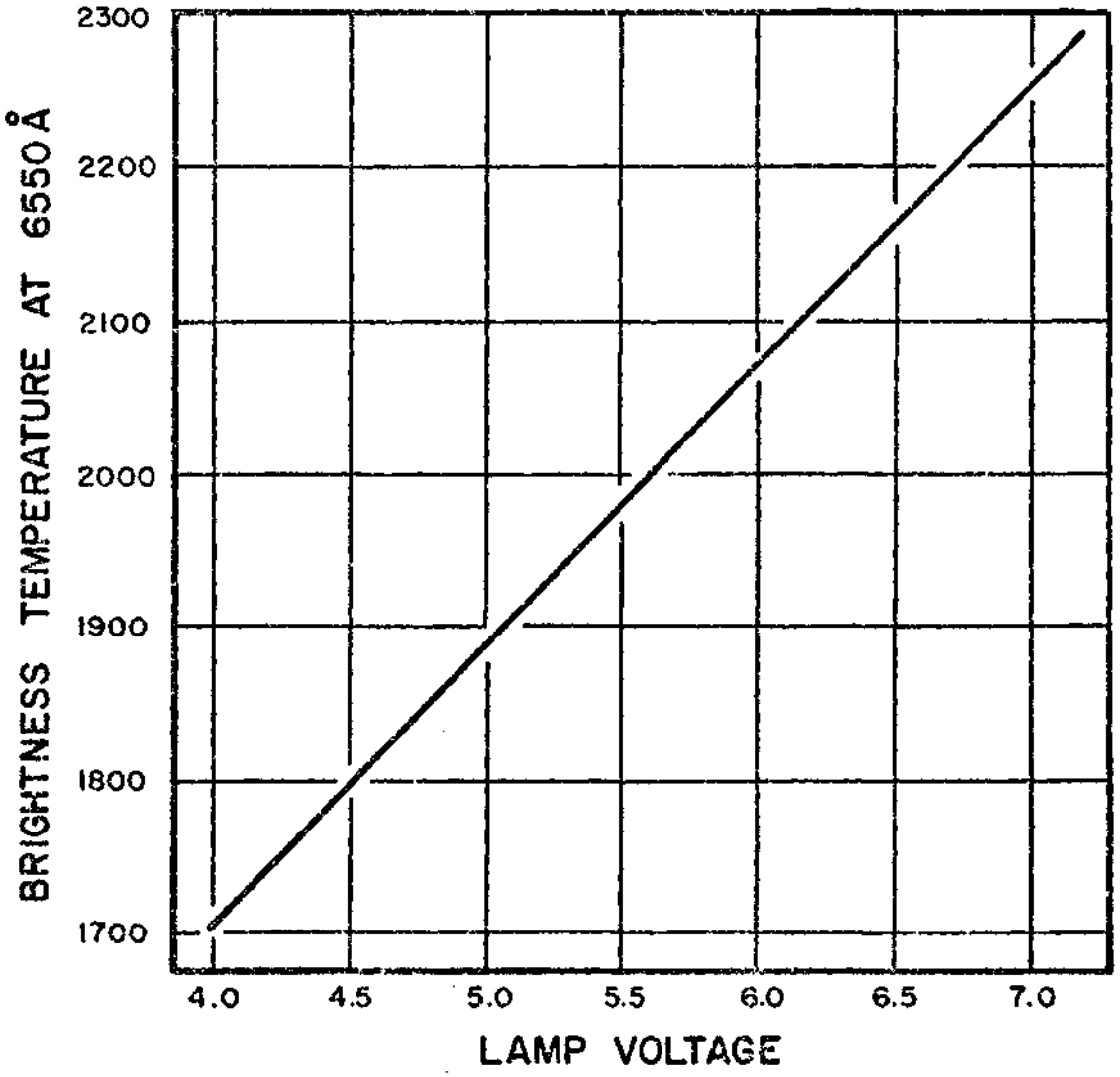

Figure A7. Reference Lamp Calibration Curve

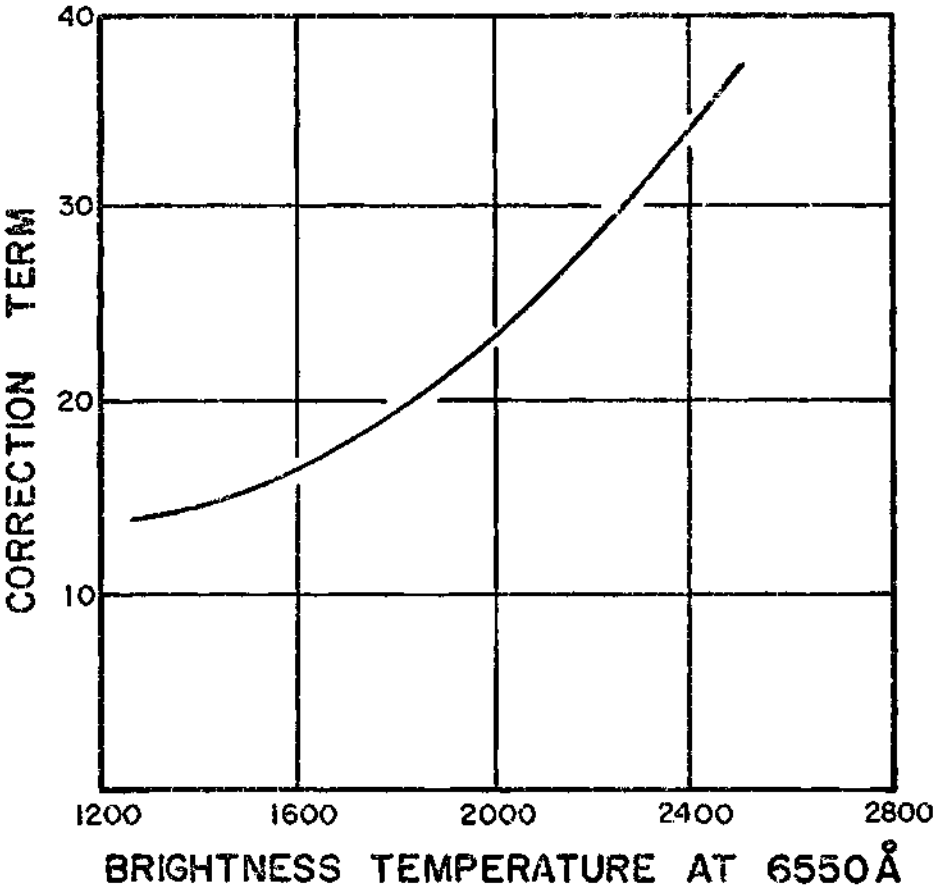

$$T_{b5893Å} = T_{b6550Å} + \text{CORRECTION TERM} \quad (°C)$$

Figure A8. Brightness Temperature Correction Curve

BIBLIOGRAPHY

LITERATURE CITED

1. Zimmer, M. F. and R. Zimmer-Galler, "Researches and Reviews of Fuels for Air Breathing Propulsion," The Performance of High Temperature Systems Vol. I, 181, Gordon and Breach, New York (1968)

2. Shakill, M. A., "Design and Preliminary Testing of a Pre-Mixed Flat Flame Burner Incorporating an Opposed Particle Jet," MS Thesis, Georgia Institute of Technology (1970)

3. Greenbaum, M. A. and M. Farber, "Studies of the Thermodynamic Properties of the Compounds of the Light Metals," The Performance of High Temperature Systems Vol. I, 1-8, Gordon and Breach, New York (1968)

4. Sprague, R. W., "Theoretical Equilibrium Corrosion of Refractory Materials by Condensed Oxides," The Performance of High Temperature Systems Vol. I, 19-32, Gordon and Breach, New York (1968)

5. Brzustowski, T. A. and I. Glassman, "Spectroscopic Investigation of Metal Combustion," AIAA Progress in Aeronautics and Astronautics: Vol. 15 Heterogeneous Combustion, 41-73, Academic Press, New York (1964)

6. Fassel, W. M., C. A. Papp, D. A. Hildebrand, and R. P. Serrka, "The Experimental Nature of the Combustion of Metallic Particles," Solid Propellant Rocket Research, 259-269, Academic Press, New York (1960)

7. Macek, A., R. Friedman, and J. M. Semple, "Techniques for the Study of Beryllium and Aluminum Particles," AIAA Progress in Aeronautics and Astronautics: Vol 15 Heterogeneous Combustion, 3-16, Academic Press, New York (1964)

8. Drew, C. M., A. S. Gordon, and R. H. Knipe, "Study of Quenched Aluminum Particle Combustion," AIAA Progress in Aeronautics and Astronautics: Vol. 15 Heterogeneous Combustion, 17-39, Academic Press, New York (1964)

9. Brzustowski, T. A., and I. Glassman, "Vapor Phase Diffusion Flames in the Combustion of Magnesium and Aliminum," AIAA Progress in Aeronautics and Astronautics: Vol. 15 Heterogeneous Combustion, 75-115, Academic Press, New York (1964)

10. Fisk, C. A., "Flat Flame Burner with an Opposed Nitrogen-Aluminum Particle Jet," MS Thesis, Georgia Institute of Technology (1971)

11. Lewis, B. and G. von Elbe, "Stability and Structure of Burner Flames," J. Chem. Physics, 11, 77 (1943)

12. Jones, G. W., B. Lewis, J. B. Friauf, and G. S. Perrott, "Flame Temperatures of Hydrocarbon Gases," J. Am. Chem. Soc., 53, 3992-4001 (1931)

13. Doty, W. I., "Modification of a Two Meter Spectrograph and Its Use in Combustion Research," MS Thesis, Georgia Institute of Technology (1969)

14. Thomas, D. L., " An Automatic Remotely Operated Sodium D Line Reversal Temperature Measuring Technique," C & F, 12, 569-574 (1968)

15. Snelleman, W., "Errors in the Method of Line Reversal," C & F, 11, 453-463 (1967)

16. Mavrodineau, R. and H. Boiteux, Flame Spectroscopy, 510-511, John Wiley & Sons, Inc., New York (1965)

17. Gaydon, A. G. and H. G. Wolfhard, "Spectroscopic Studies of Low Pressure Flames. IV. Measurements of Light Yield for C_2 Bands," Proc. Roy. Soc. London, A201, 570-586 (1950)

18. Griffiths, E. and J. W. Awberry, "The Measurement of Flame Temperature," Proc. Roy. Soc. London, A123, 401-425 (1929)

19. Henning, F. and C. Tingwaldt, "The Temperature Distribution in the Acetylene Welding Flame," Z. Ver. Deut. Ing., 72, 1828-1830 (1928)

20. Schmidt, H., "Verification of the Radiation Laws in a Bunsen Flame," Ann. Phys., 29, 971-1028 (1909)

21. Kohn, H., "Mechanism of Radiation from Metallic Vapors in Flames," Ann. Phys., 34, 749-782 (1914)

22. Broida, H. P. and K. E. Shuler, "Spectroscopic Study of Electronic Flame Temperatures and Energy Distributions," J. Chem. Phys. 27, 933-939 (1957)

23. Tourin, R. H., Spectroscopic Gas Temperature Measurement, Elsevier Publishing Co., New York (1966)

24. Bundy, F. P. and H. M. Strong, "Measurements of Temperatures in Flames of Complex Structure by Resonance Line Radiation," J. App. Phys., 25, 1521-1537 (1954)

25. Forsyth, W. E., "Optical Pyrometry," Temperature: Its Measurement and Control in Science and Industry, 1115-1131, Reinhold Publishing Co., New York (1941)

26. Fluid Meters: Their Theory and Application, Report of the ASME Research Committee on Fluid Meters, S. R. Beitler, Chairman, 87, ASME, New York (1959)

ADDITIONAL REFERENCES

Brode, W. R., Chemical Spectroscopy, 2nd Ed., John Wiley & Sons, Inc., New York (1947)

Fristrom, R. M. and A. A. Westenberg, Flame Structure, McGraw Hill, New York (1965)

Gaydon, A. G. and H. G. Wolfhard, Flames: Their Structure, Radiation, and Temperature, 3rd Ed., Chapman and Hall, London (1970)

Lewis, B. and G. von Elbe, Combustion Flames and Explosions of Gases, 2nd Ed., Academic Press, New York (1961)

Sawyer, R. A., Experimental Spectroscopy, 3rd Ed. Dover, New York (1963)